Article

Exploring two-photon optogenetics beyond 1100 nm for specific and effective all-optical physiology

tuning spike detection to 100% specificity

combining 2P resonant imaging with 2P raster scan optogenetics in mouse V1

GCaMP6f C1V1

calcium imaging 920 nm

2P stimulation 1020 - 1300 nm

artifact free all-optical physiology beyond 1100 nm

no further increase in efficacy until 1300 nm

Ting Fu, Isabelle Arnoux, Jan Döring, ..., Ignas Stasevicius, Wei Fan, Albrecht Stroh

albrecht.stroh@unimedizin-mainz.de, jan-michael.doering@charite.de

HIGHLIGHTS

We developed an algorithm for 100 %-specific identification of AP-related calcium transients

Artifact-free all-optical experiments can be achieved from 1100 nm to 1300 nm

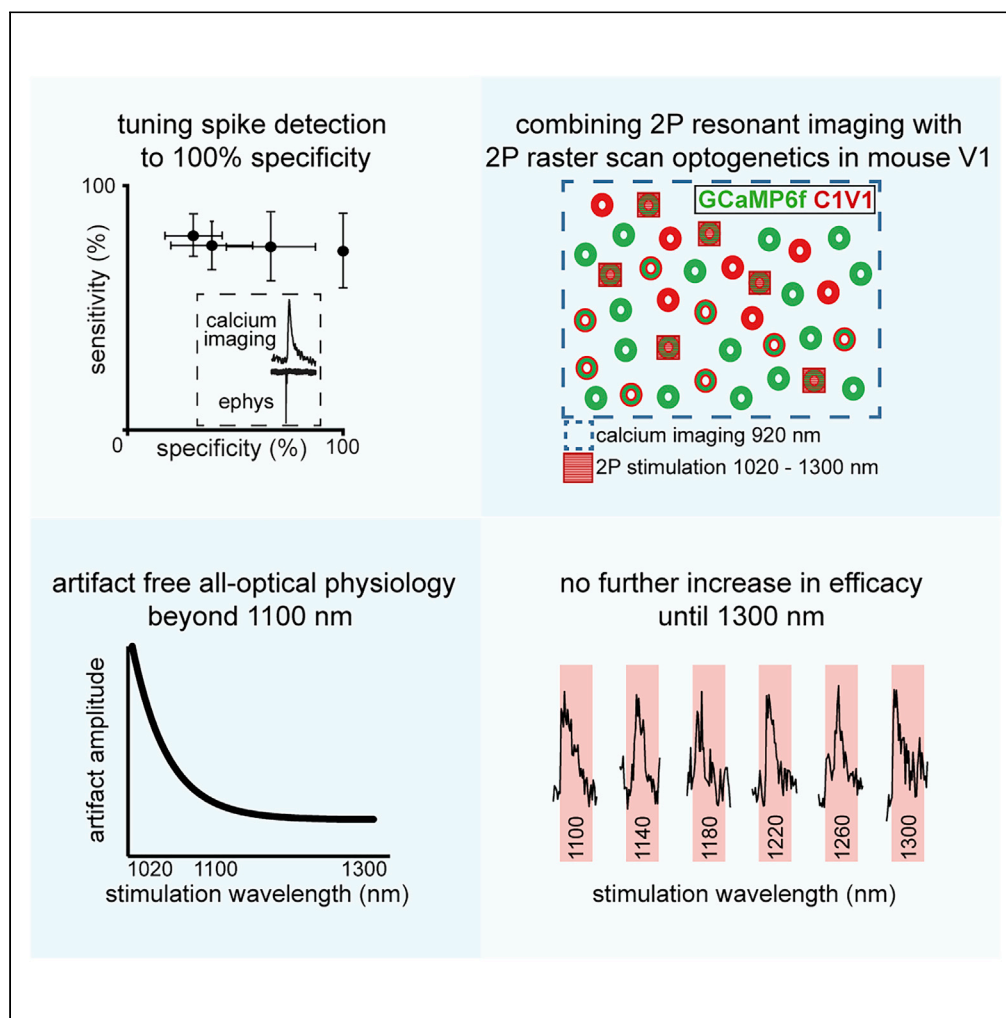Efficacy of C1V1 excitation does not increase beyond 1100 nm until 1300 nm

Article

Exploring two-photon optogenetics beyond 1100 nm for specific and effective all-optical physiology

Ting Fu,[1,2,6] Isabelle Arnoux,[1,3,6] Jan Döring,[1,6] Hendrik Backhaus,[2] Hirofumi Watari,[1] Ignas Stasevicius,[4,5] Wei Fan,[1,2] and Albrecht Stroh[1,2,7,*]

SUMMARY

Two-photon (2-P) all-optical approaches combine *in vivo* 2-P calcium imaging and 2-P optogenetic modulations. Here, firstly, we combined *in vivo* juxtacellular recordings and GCaMP6f-based 2-P calcium imaging in mouse visual cortex to tune our detection algorithm towards a 100% specific identification of action potential-related calcium transients. Secondly, we minimized photostimulation artifacts by using extended-wavelength-spectrum laser sources for optogenetic stimulation. We achieved artifact-free all-optical experiments performing optogenetic stimulation from 1100 nm to 1300 nm. Thirdly, we determined the spectral range for maximizing efficacy until 1300 nm. The rate of evoked transients in GCaMP6f/C1V1-co-expressing cortical neurons peaked already at 1100 nm. By refining spike detection and defining 1100 nm as the optimal wavelength for artifact-free and effective GCaMP6f/C1V1-based all-optical physiology, we increased the translational value of these approaches, e.g., for the development of network-based therapies.

INTRODUCTION

In vivo two-photon (2-P) all-optical approaches are based on simultaneous 2-P optogenetic modulations and 2-P calcium imaging (Emiliani et al., 2015). They allow for causal interrogations of neuronal networks on single-cell level in a minimal-invasive fashion by using spatially confined light for readout and manipulation. In recent years, 2-P-based methods have been successfully employed for all-optical control of neural microcircuits *in vivo* (Rickgauer et al., 2014; Packer et al., 2015; Carrillo-Reid et al., 2016; Forli et al., 2018; Mardinly et al., 2018; Zhang et al., 2018; Carrillo-Reid et al., 2019; Chen et al., 2019; Marshel et al., 2019). Using parallel (Rickgauer et al., 2014; Mardinly et al., 2018; Chen et al., 2019) or hybrids of parallel and scanning methods (Packer et al., 2012; Yang et al., 2018a; Zhang et al., 2018; Carrillo-Reid et al., 2019; Marshel et al., 2019), mainly involving different variants of computer generated holography (CGH), volumetric imaging of hundreds of neurons across cortical layers and simultaneous manipulation of neuronal ensembles with dozens of neurons became feasible (Carrillo-Reid et al., 2016; Mardinly et al., 2018; Yang et al., 2018a; Marshel et al., 2019). Lately, the revolutionizing concept of all-optical physiology has been successfully applied to modulate complex behavior in mammals (Carrillo-Reid et al., 2019; Marshel et al., 2019) and was extended to closed-loop designs (Zhang et al., 2018). However, although these approaches are advancing rapidly, important aspects concerning specificity and efficacy have not been sufficiently addressed, yet.

Utmost specificity and sensitivity are of crucial importance for applications of all-optical approaches in the context of preclinical research in animal models of neurological disorders. Employing all-optical approaches in this field is not farfetched as the combination of 2-P calcium imaging and 2-P optogenetic stimulation would (a) allow us to detect individual dysregulated neurons (Busche et al., 2012; Arnoux et al., 2018; Ellwardt et al. 2018) and would (b) allow us to modulate their activity in a highly specific manner, e.g., by silencing hyperactive neurons, while leaving intact network components untouched. However, in *in vivo* imaging experiments optical signals are inherently noisy and only indirectly mirroring neuronal activity. Deflections in the fluorescent trace are not only caused by the underlying neurophysiological signal of interest but can be due to movement or non-physiological artifacts, e.g., stimulation light can cause a deflection in

the calcium trace when stimulation and imaging channels are not spectrally well separated, as well as ambient light when the preparation is not well shielded from light sources in its surrounding.

On the detection, ultimately, 2-P calcium imaging does not provide a direct readout of neuronal activity, unlike electrophysiology (Stosiek et al. 2003). It reports—at the level of microcircuits—the fast elevation of intracellular calcium levels upon action potential (AP) firing (Grienberger and Konnerth 2012). Consequently, the first task toward a specific detection of the optical correlate of APs represents the specific identification of these stereotypical calcium transients. The second task towards a specific all-optical physiology represents the avoidance of optical non-AP-related artifacts and the cross talk between imaging and stimulation. While, e.g., movement artifacts strongly depend on the quality of preparation, stimulation artifacts are experimenter independent, as they are caused by cross talk between imaging and stimulation channels. A further important issue, which has not been comprehensively addressed, yet, concerns the spectral efficacy of optogenetic control. The spectral range for effective optogenetic control has still not been thoroughly defined. Studies in slice preparations suggest an increase in photocurrents with increasing wavelength; however, the maximum wavelength was limited to 1080 nm (Prakash et al. 2012; Marshel et al., 2019). Until now, no actuator has been tested using wavelengths beyond this range, mainly due to technical limitations.

Here, we propose a step-by-step approach tackling these aforementioned limitations: (I) we provide data on the sensitivity of 2-P calcium imaging in terms of specific, false-positive-free identification of AP-related calcium transients, (II) we determine the spectral window for artifact-free stimulation, and, lastly, (III) we assess the efficacy of opsin stimulation beyond 1100 nm.

RESULTS

Implementing a highly specific optical detection of neural spiking activity in cortical circuits

For the application of optical imaging of cortical microcircuit dynamics, i.e., the optical correlate of APs, high specificity combined with high sensitivity is paramount. We have developed a program suite comprising different analysis tools (Arnoux et al., 2018), which take into account the rather stereotypical dynamics of an AP-related calcium transient such as the dynamics of its rise, its duration, and its decay (see Transparent methods Arnoux et al., 2018). This is of particular importance, as a mere deflection of the calcium traces from the baseline could very well have non-AP-related origins, such as motion or light artifacts. To test for the specificity and sensitivity of its built-in peak detection algorithm, here, we conducted simultaneous juxtacellular electrophysiological recordings and 2-P calcium imaging in the visual cortex of the lightly anesthetized mouse. For that, we performed viral-based gene transfer of the genetically encoded calcium indicator GCaMP6f in cortical neurons. In these bimodal recordings, a stable calcium trace with large-scale deflections could be observed (Figures 1A and 1B). This calcium trace was synchronized with the juxtacellular recordings in voltage clamp mode, displaying typical sparse spontaneous AP firing (Rochefort et al. 2009). We set the peak detection criteria in a way that no false positives, i.e., detection of calcium peaks in the absence of temporally locked APs, were identified (Figure 1B). It has to be noted that, indeed, simply correlating relative fluorescence changes with, e.g., the behavioral context, without taking into account the typical temporal dynamics of AP-related calcium transients would have led to the false identification of calcium transients being related to APs. Keeping the specificity at 100%, the average sensitivity of our transient detection was 73 ± 15% (Figure 1C). Of note, a detection of the optical correlate of single APs was not achieved, employing this rigorous analysis aimed for maximizing specificity, even though we used state-of-the-art optics and indicators with high expression levels. For achieving single-action potential resolution requires optimal imaging conditions, with a low baseline noise, low movement particularly in z-direction, and high specific expression of the indicator. By comparing the automated transient identification used in our study with current state-of-art techniques, such as OASIS (Online Active Set method to Infer Spikes), we obtained a higher sensitivity employing the OASIS deconvolution approach in comparison to our algorithm (Figure S1A). But, and this is critical, this comes at a cost of lower specificity, i.e., a significant portion of false positives. The likelihood to identify an AP-related calcium transient increased with the number of APs exhibited by the GCaMP6f-positive neuron (Figure 1D) resulting in converging curves for AP and transient detection at higher firing rates (Figure 1E). To test whether line scanning at 920 nm for imaging of GCaMP6f impacts neuronal physiology, e.g., by heating the brain tissue, we compared firing rates between periods of scanning and periods when the scanner was off (Figures 1F and 1G). Notably, using typical light intensities of 10–30 mW in resonant imaging mode with a pixel dwell time of 1 μs, we did not observe a significant change in the spiking rate between periods of scanning and non-
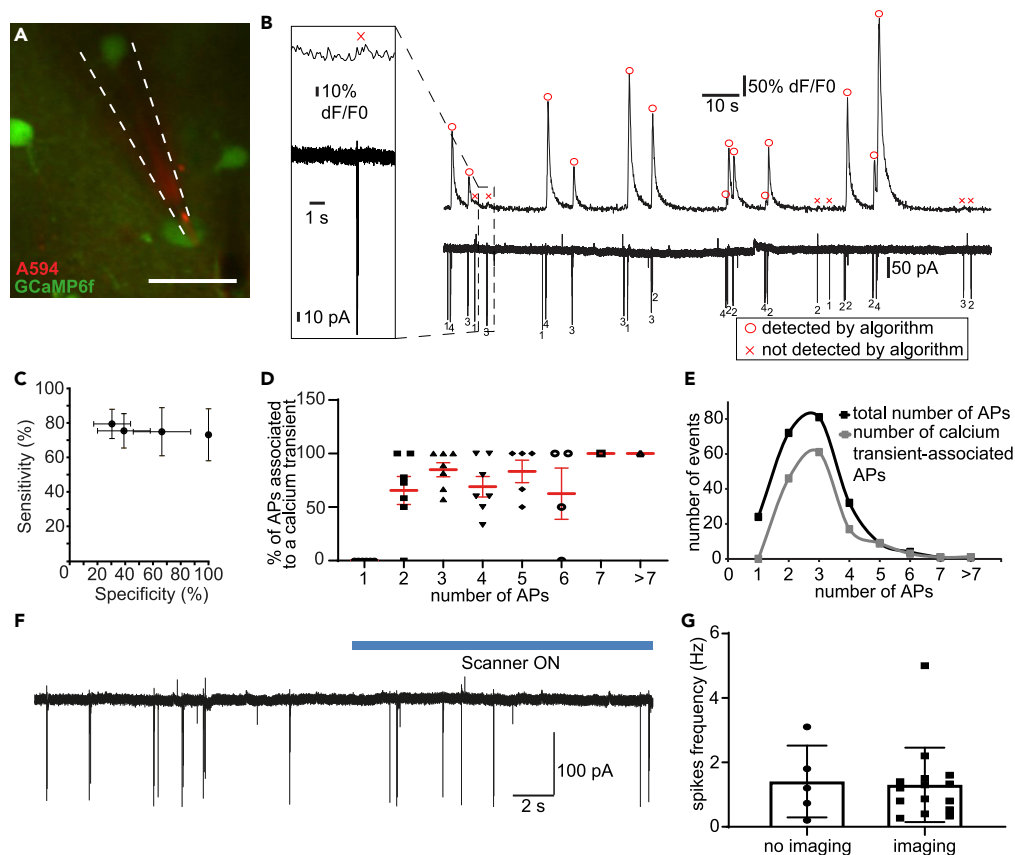
Figure 1. Implementing a highly specific optical detection of neural spiking activity in cortical circuits

(A) Simultaneous 2-P imaging and juxtacellular recordings of GCaMP6f-expressing neuron (green). Patch pipette filled with AlexaFluo594 (red), scale bar: 20 μm.

(B) Spontaneous activity of a GCaMP6f-expressing neuron. Calcium trace acquired with 2-P imaging (upper) and current trace (lower) obtained by juxtacellular recording of the same neuron. AP-associated calcium transients as detected by the algorithm are marked by a red circle. APs not accompanied by detected calcium transients are marked by a red cross in the calcium trace. Numbers of APs are indicated below the trace.

(C) Sensitivity and specificity for calcium transient detection based on the chosen standard deviation threshold. Applying a threshold of 0.05 standard deviation (SD) results in a mean sensitivity of 80 ± 9%, reaching a specificity of 30 ± 13%. An increase of the threshold to 0.2, 0.5 SD, and 1 SD is reducing the sensitivity to 75 ± 10%, 75 ± 14%, and 73 ± 15% respectively. The corresponding specificity for an SD threshold of 0.2 and 0.5 increases to 40 ± 19% and 66 ± 21%, respectively; a threshold of 1 SD reaches 100% specificity (n = 7 neurons, 3 mice).

(D) Relation of APs associated to a detected calcium transient to all detected APs, n = 7 neurons, 3 mice.

(E) Histogram of APs (black) and detected calcium transient-associated APs (gray), n = 7 neurons, 3 mice.

(F) Representative current trace without and with (indicated by blue line above) line scanning in resonant mode at 920 nm.

(G) Analysis of spikes frequency w/o 2-P resonant scanning. n = 7 neurons, 3 mice ($p = 0.84$, unpaired t test with Welch's correction).

Data are represented as mean ± SD. Significance levels were *$p < 0.05$, **$p < 0.01$, ***$p < 0.001$ and ****$p < 0.0001$.

scanning. In conclusion, while achieving high specificity comes at a cost, we could still capture above 70% of all electrophysiologically detected APs.

Functional calcium transients can only be detected in a rather narrow spectral window

For an all-optical experiment with minimal cross talk, it is essential to spectrally separate imaging and stimulation. Therefore, we needed to define the spectral window allowing for the reliable detection of functional calcium transients as done before (Akerboom et al. 2012). We performed *in vivo* imaging of GCaMP6f-expressing neurons at different wavelengths of the same field of view, again in layer II/III of visual cortex in lightly anesthetized mice (Figure S1B). First, we investigated the shortest wavelength allowing for the identification of individual GCaMP6f-expressing neurons. The number of visually detectable neurons

was similar across wavelengths ranging from 860 to 920 nm (Figure S1B). Therefore, 860 nm was still in the pumping spectrum of the optical parametric oscillator (OPO, see below) and therefore might allow a system based on one laser source. However, while the neurons could be clearly identified, below 880 nm hardly any functional transient was detectable ($18.3 \pm 3.6\%$, Figure S1D). At 880 nm, a minor fraction ($27.6 \pm 10.0\%$) and at 900 nm, less than half of the transients could be recorded ($48.8 \pm 10.6\%$) compared to imaging at 920 nm, where the number of detected calcium transients increased substantially (Figures S1C and S1E). Likewise, the number of detectable active cells increased in similar fashion when increasing the imaging wavelength from 860 to 920 nm ($18.3 \pm 3.6\%$ at 860 nm, $27.6 \pm 9.9\%$ at 880 nm, $49 \pm 11\%$ at 900 nm, $100 \pm 0\%$ at 920 nm, Figure S1D). Also, spontaneous transient frequencies increased significantly from 860 to 920 nm (0.33 ± 0.1 transients/min at 860 nm, 1.17 ± 0.29 transients/min at 880 nm, 1.33 ± 0.23 transients/min at 900 nm, 1.69 ± 0.22 transients/min at 920 nm, Figure S1F). Consequently, we could replicate that the spectral window for the detection of functional calcium transients is significantly smaller than the window for the morphological identification of GCaMP6f-expressing neurons (Akerboom et al. 2012).

Implementations of spectrally independent 2-P light sources

As the lower edge of the spectral range for our all-optical experiments was now set to 920 nm due to the functional limitations of GCaMP6f discussed above, we had to devise a light source, which flexibly delivered longer wavelengths for cross talk-free optogenetic modulations. Previous work on all-optical physiology used fixed-wavelength ytterbium lasers typically between 1040 and 1080 nm for the 2-P excitation of opsins. We chose to probe whether longer wavelength might both reduce cross talk and improve efficacy.

For achieving this goal, several technical solutions are amenable: One conceivable approach is to use one tunable 2-P Ti:Sa laser source and splitting the beam power for pumping an OPO and for imaging GCaMP6f (Figure S2A). However, 920 nm, the wavelength for functional GCaMP6f imaging, is well beyond the pumping spectrum of most OPO models. In this configuration, the system could therefore only be used in combination with indicators effectively excitable with lower wavelengths, such as Oregon-Green-BAPTA 1, excitable at 800 nm. For all-optical experiments reported in this study, based on GCaMP6f, we probed two different configurations both based on two primary laser sources: The first configuration integrates a second 2-P tunable Ti:Sa laser. One of the two independently tunable beams is dedicated for imaging, allowing full Ti:Sa-spectrum (680–1060 nm), and the other Ti:Sa is set at the optimal wavelength for pumping the subsequent OPO, resulting in full OPO spectrum (1100–1400 nm) for optogenetic stimulation (Figure S2B). The second configuration comprises a single femtosecond laser with two independently tunable output channels simultaneously emitting two beams for imaging (680–960 nm) and stimulation (950–1300 nm) (Figure S2C). Each channel's maximum output power exceeds 1 W. In both configurations, we temporally uncoupled dwell times of the excitation and imaging beams using separate lasers and scanners for imaging and stimulation. This is important, as the pixel dwell time achieved in resonant scanning mode is in the nanosecond range and therefore not sufficient for effective excitation of an opsin, mandating more than 4 µs (Prakash et al. 2012). Consequently, only the 2-P beam used for imaging was coupled to the fast resonant scanner, and the second longer wavelength was coupled to an additional galvanometric scanner. To achieve a high spatial specificity in modulating activity of single cells, it is crucial that the excitation volume is confined and does not exceed the spatial extent of the neuron supposed to be stimulated. Only then, specific scanning patterns can be applied to, e.g., specifically target neurons showing aberrant activity without interfering the activity of well-functioning neighboring network components. The excitation volume of individual microscope systems is defined by their point spread function (PSF), and 2-P illumination theoretically allows excitation of femtoliter volumes. At 920 nm, the PSF of our system had an acceptable full width half maximum (FWHM) of 0.20 ± 0.03 µm in x and 0.26 ± 0.01 µm in y-direction, while the FWHM in z-direction was approximately 1.60 ± 0.05 µm (Figure S2F). These measurements were stable using different excitation wavelengths (Figures S2D–S2F) and allowed to concentrate the excitation on a 0.08 µm^3 volume (Figure S2E). In these configurations, our 2-P system was therefore capable of performing spatially specific and spectrally independent optogenetic modulations temporally uncoupled from high-speed GCaMP6f imaging.

Probing functional co-expression of indicator and actuator applying 1- and 2-P optogenetic stimulation

For highly specific all-optical interrogations combining precise optogenetic control and optical readout from individual neurons, the indicator and the opsin protein need to be co-expressed in the neuronal population of interest. We therefore co-injected two Adeno-associated virus (AAV)-based viral vectors encoding for the 2-P excitable opsin C1V1$_{T/T}$ and the calcium indicator GCaMP6f. We titrated both viruses to achieve strong co-expression of both sensor and actuator protein by examining different dilutions of

each virus. When increasing the titer of either AAV, we could observe a predominant expression of either GCaMP6f or C1V1$_{T/T}$-mCherry due to the limited protein synthesis capacity of single neurons (Figures S3A–S3F). Hence, viral vector-based schemes for transduction of postmitotic neurons with opsin and indicator require careful titration. If a given titer is effective for strong expression of the indicator, the second virus encoding the opsin cannot be simply added, as this might lead to overexpression-mediated apoptosis (Aschauer et al. 2013; Yang et al., 2018b).

Stable co-expression of C1V1$_{T/T}$ and GCaMP6f could be observed in confocal analysis of the tissue sections employing a final titer of 20:1 for C1V1$_{T/T}$ (3.33 * 10^{11}/mL) and GCaMP6f (1.84 * 10^{10}/mL) (Figures 2A and S4). Using this titer, the density of C1V1$_{T/T}$-mCherry-positive cells was 1392 $\pm$ 97 cells/mm^3 in layer II/III and 4336 $\pm$ 313 cells/mm^3 in layer V/VI. The density of cells co-expressing C1V1$_{T/T}$-mCherry and GCaMP6f was 735 $\pm$ 99 cells/mm^3 in layer II/III and 1226 $\pm$ 139 cells/mm^3 in layer V/VI resulting in a fraction of 52.5 $\pm$ 4.4% and 28.3 $\pm$ 2.3% of C1V1$_{T/T}$/GCaMP6f co-expressing cells in layer II/III and in layer V/VI, respectively. Hardly any co-expressing neurons were found in layer IV. We found strong and dense co-expression across targeted cortical layers II/III and V/VI. Note that layer IV seems to be difficult to target with AAVs of serotype I/II, as reported previously (Schmid et al. 2016; Yang et al. 2017).

Electrophysiological recordings provide a direct readout of neuronal activity and are therefore well suited to probe functionality of opsin expression and test 2-P excitation paradigms. To ensure functional expression of our optogenetic actuator, we therefore performed easy to implement optic fiber-based 1-P stimulations at 552 nm in combination with local field potential LFP recordings ((Fois et al. 2014), Figures 2B and 2C). Within single animals, we found a stable response pattern with a low variability of response amplitudes at approximately 60 mW/mm^2 (Figure 2D). However, between animals amplitudes varied, with an average amplitude of 11.9 $\pm$ 0.4 mV. Next, in a proof-of-principle experiment we tested whether our 2-P light source in combination with a raster scan paradigm was capable of eliciting spikes in individual opsin expressing neurons (Figure S3G). Simultaneous juxtacellular recordings demonstrated stable responses upon every trial of single-cell 2-P optogenetic stimulations with a light intensity of 37 mW at 1100 nm (Figures S3H and S3I). We applied a pixel dwell time of 6 µs with a raster width of 0.5 µm. Like this, specific modulations of single neurons were achievable by applying our stimulation approach with a success rate of 100% using light intensities $\geq$ 37 mW in 26 consecutive trials (96% at 18 mW, Figure S3M). Latencies decreased with increasing light intensities (Figure S3J), as reported previously (Stroh et al. 2013), while photocurrents increased (Figure S5L). Interestingly, light intensities $\leq$ 37 mW only triggered approximately one event whereas light intensities around 60 mW already triggered two events (Figure S3K). This is important to note as for low AP numbers the sensitivity of our peak detection algorithm is decreasing substantially. Thus, we decided to perform our stimulations in imaging experiments at light intensities $\geq$ 40 mW. In summary, these quality control and feasibility experiments provide the needed foundation for subsequent all-optical experiments.

Above noise stimulation artifacts of 2-P excitation are wavelength dependent and absent above 1100 nm

Unlike electrophysiological recordings, optical imaging using genetically encoded calcium indicators does not provide a specific signal per se. Identification of AP-derived calcium transients critically depends on several components of the signal, such as the sharp rise time. An artifact of the stimulation pulse in the GCaMP6f emission channel renders a highly specific identification of AP-related calcium transients difficult. This is of particular concern, if this method is applied in preclinical research, which should provide evidence guiding translation to human studies (Duda et al. 2014; Dirnagl 2016, 2019; Piper et al. 2019). Here, we defined the spectral windows for artifact-free all-optical interrogations by testing different wavelengths for stimulation. To ensure that photostimulation artifacts were in fact no mistaken calcium transients, we performed our stimulation paradigm on mice which were lacking C1V1 expression and solely expressed GCaMP6f (Figure 3A). Notably, applying stimulation wavelengths and power used for all-optical experiments (Packer et al. 2015; Yang et al., 2018a; Carrillo-Reid et al. 2019; Marshel et al., 2019), we observed a significant artifact in the calcium trace when stimulating at 1020 nm, already at 40 mW power (Figure 3B). Increasing power levels to 80 mW which increases the efficacy of stimulation led to even more pronounced artifacts (Figures 3B and 3C). Note that this artifact displayed a sharp rise time and an amplitude well above the noise level so that it might be misinterpreted as an AP-related calcium transient. Also, the amplitude of the artifact varied drastically between trials, rendering automated subtraction of mean artifacts, as conducted in a previous study using single-wavelength all-optical physiology, obsolete (Schmid et al. 2016). To define the spectral range for artifact-free all-optical physiology, we now increased the stimulation
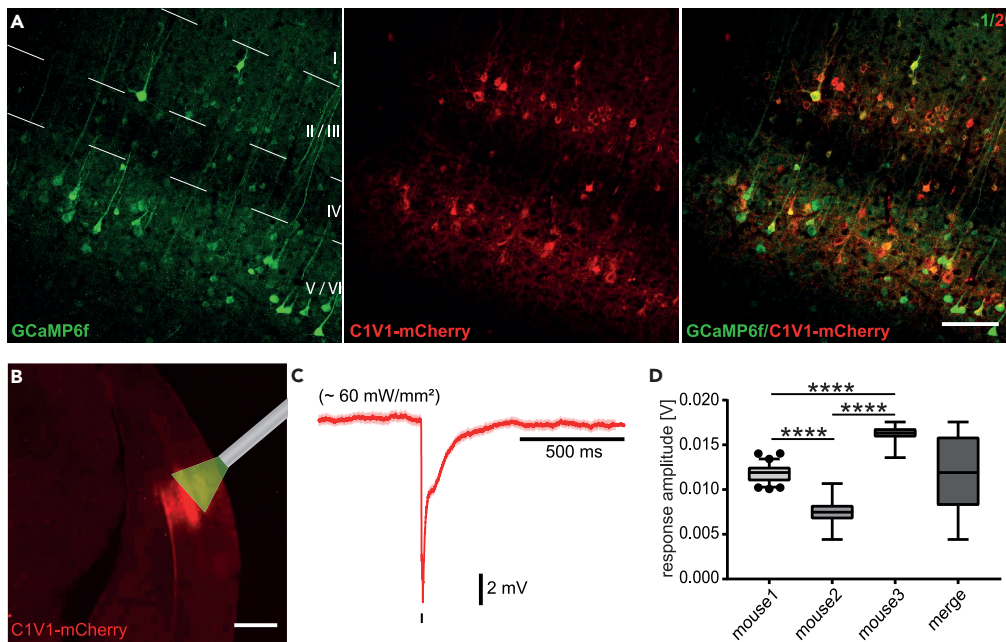
Figure 2. Achieving strong co-expression of actuator and indicator and probing functional expression

(A) Confocal micrographs of co-expression pattern in the primary visual cortex. Left: green channel at 488 nm. Middle: red channel at 584 nm. Right: overlay. Scale bar: 75 μm.

(B) Epifluorescence micrograph of typical C1V1$_{T/T}$-mCherry expression and schematic inset of the optic fiber for 1-P stimulation at 552 nm. Scale bar: 500 μm.

(C) Average LFP response upon optogenetic stimulation at 60 mW/mm^2, n = 31 responses.

(D) Average LFP response amplitudes upon stimulations at 60 mW/mm^2 (unpaired t: test mouse 1 vs mouse 2 p < 0.0001, Mann-Whitney test: mouse 1 vs mouse 3 p < 0.0001, mouse 2 vs mouse 3 p < 0.0001, n = 31 responses each, 3 mice). Data are represented as mean ± SEM (standard error of the mean). Significance levels were *p < 0.05, **p < 0.01, ***p < 0.001 and ****p < 0.0001.

wavelength step by step. We found that the amplitude of the averaged and normalized artifact decreased with increasing wavelength (Figure 3D). At 1060 nm, again, often used in ytterbium-laser-based 2-P opto-genetics, an artifact was still clearly visible beyond noise level (Figures 3D and 3E). Above 1100 nm, the amplitude of the stimulation artifact was greatly reduced and within the noise level (Figures 3D and 3E). Above 1100 nm, the artifact amplitude stayed approximately constant in the tested wavelength spectrum up to 1300 nm. In summary, it has to be stated that the artifacts induced by photostimulation were highly heterogeneous in shape and amplitude. This might be explained by unintended excitation of GCaMP's fluorescent core eGFP and varies with varying expression levels of the reporter and varying levels of auto-fluorescence. We suggest using wavelengths of 1100 nm or higher for artifact-free all-optical physiology.

Optimal wavelength for effective and cross talk-free optogenetic control in C1V1/GCaMP6f-based experimental approaches is 1100 nm

Finally, we conducted *in vivo* experiments in animals expressing high and functional levels of both opsin and indicator in the lightly anesthetized mouse. First, we performed GCaMP6f imaging only. We assessed simultaneously the full-field activity of the local ensemble of neurons. We set the anesthetic depth in a way that persistent, desynchronized population activity could be observed (Figures S4A and S4B). Deeper anesthesia will result in slow-wave-brain state, which is characterized by large amplitude oscillations (Figures S4A and S4B). This brain state would not be suitable for probing the excitability and connectivity of each neuron, as the excitability of the respective neuron would be governed by the current phase of the population-wide oscillation (Schwalm et al., 2017). In persistent brain state, we next carried out cell-specific interventions on genetically defined C1V1$_{T/T}$-expressing neurons using 2-P-based optogenetic stimulation. We carried out sequential stimulations of individual cells at the artifact-free wavelength of 1100 nm using aforementioned raster scans while simultaneously imaging GCaMP6f fluorescence at 920 nm (Figure 4A). The performed stimulation paradigm robustly elicited putatively AP-related GCaMP6f transients
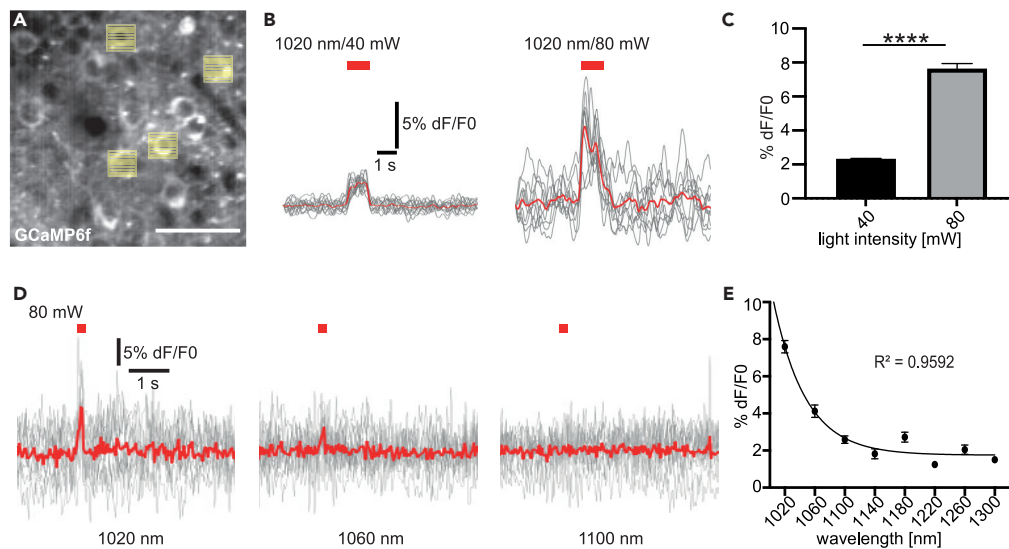
Figure 3. Stimulation artifact of 2-P excitation is wavelength dependent and absent above 1100 nm

(A) *In vivo* 2-P calcium imaging of GCaMP6f expressing neurons in layer II/III of the mouse visual cortex and simultaneous raster scan stimulations of selected cells at different wavelengths and light intensities. Please note the photostimulation artifact (white vertical lines). Scale bar: 50 μm.

(B) Average artifacts (red line, n = 10 artifacts, single trials are depicted in gray) in calcium traces of selected neurons upon 40 and 80 mW raster scan stimulations at 1020 nm. The amplitude of the artifact is increasing with increasing stimulation light power.

(C) Quantification of artifact amplitude at 40 and 80 mW. Mann-Whitney test: 40 mW vs 80 mW p < 0.0001. 40 mW n = 1192 trials, 3 mice, 80 mW n = 790 trials, 5 mice.

(D) Averaged artifact (red lines, n = 10 artifacts, single trials are depicted in gray) upon 2-P raster scan stimulations (80 mW) at varying stimulation wavelengths (1020, 1060, and 1100 nm).

(E) Quantification of artifact amplitudes at varying stimulation wavelengths at 80 mW light intensity. Average artifact amplitudes are decreasing with increasing wavelength. Please note that the stimulation artifact ranges within the noise level beyond 1100 nm. Non-linear regression with a monoexponential function (R^2 = 0.96) (733–788 artifacts/wavelength, n = 5 mice).

Data are represented as mean ± SEM. Significance levels were *p < 0.05, **p < 0.01, ***p < 0.001 and ****p < 0.0001.

in stimulated cells, applying the highly specific detection algorithm implemented above at different power (210 mW: Figure 4B; 80 mW: Figure S4C). We now asked whether increasing stimulation wavelengths beyond 1100 nm, not being possible with standard Ti:Sa or ytterbium lasers, will lead to an increased efficacy. As stated above, the early studies in the field revealed a linear increase in photocurrents, until the technical limit of 1040 nm (Prakash et al. 2012). It has to be noted, however, that these studies were conducted in slice preparations, with a drastically different inhibitory tone. As the main goal of this methodological pipeline is testing the limitations and prospects of 2-P all-optical physiology in preclinical *in vivo* applications, we believe that measuring the capability of evoking detectable and specific AP-associated calcium transients represents the most appropriate avenue. Surprisingly, we found that a further increase of the stimulation wavelength from 1100 up to 1300 nm did not yield a significant increase in the rate of evoked calcium transients (Figure 4C), as well as no significant increase in the fraction of responding cells (Figure 4D). However, increasing stimulation power from rather low values ranging at 40 or 80 mW up to values ranging at 120 or 210 mW significantly increased the rate of evoked transients 2–3 fold (Figure 4E, 26.7 ± 6.7% at 40 mW, 21.6 ± 3.5% at 80 mW, 56.7 ± 13.1% at 120 mW, 76.3 ± 7.3% at 210 mW).

DISCUSSION

In this study, we provide a methodological and conceptional framework for a highly specific all-optical physiology approach. For that, challenges had to be overcome in devising a light source for spectrally independent imaging and optogenetics. Here, we used a dual-scanner approach, which is well suited for establishing this framework. In our view, holographic or combined holographic and scanning approaches based on spatial light modulators (Packer et al. 2015; Carrillo-Reid et al. 2016; Yang et al., 2018a; Carrillo-Reid et al. 2019; Marshel et al., 2019), temporal focusing (Rickgauer et al. 2014; Chen et al. 2019), or
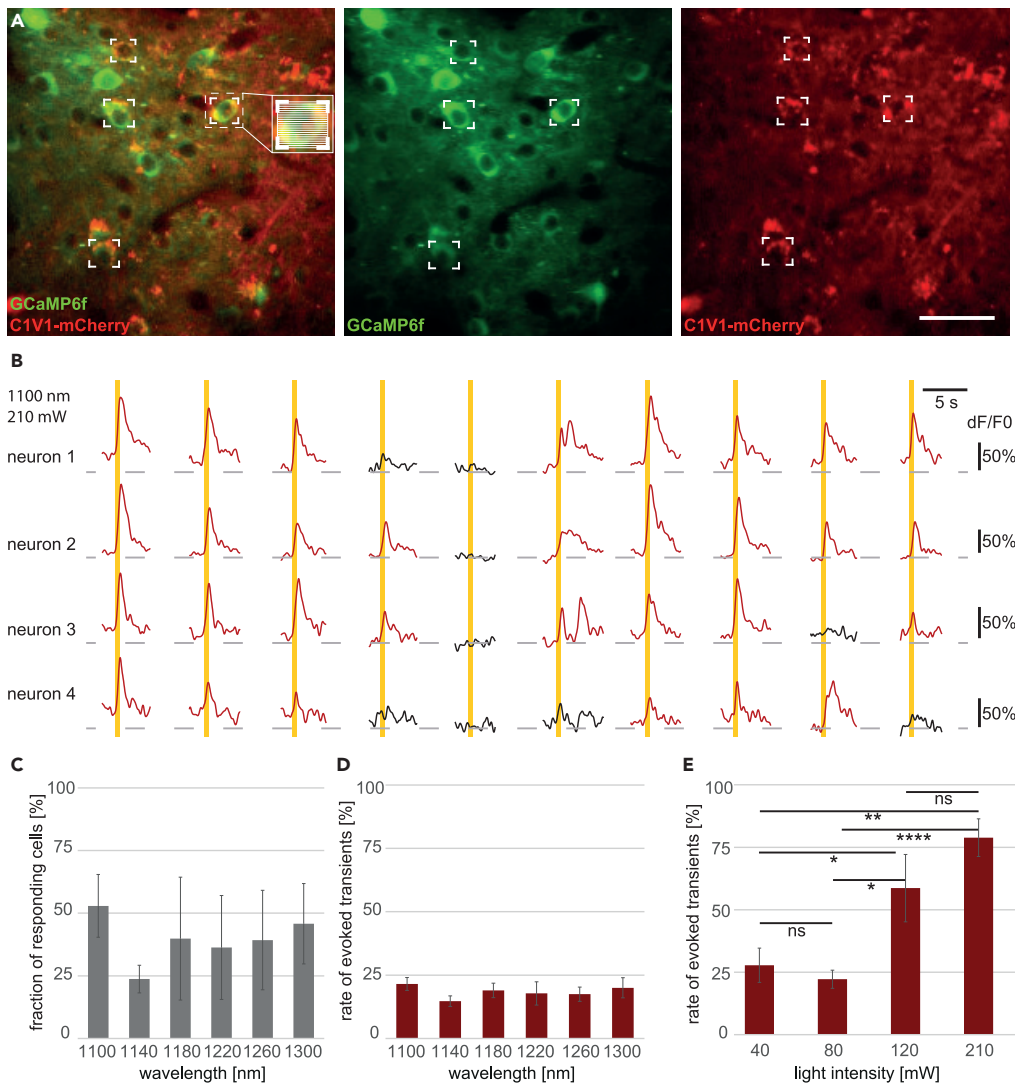
Figure 4. The optimal wavelength for effective and cross talk-free optogenetic control is 1100 nm

(A) All-optical control of individual GCaMP6f (green)/C1V1$_{T/T}$ (red) co-expressing neurons in layer II/III of mouse visual cortex. Depiction of raster scan patterns as described above. Six individual neurons can be targeted for sequential photostimulation. Scale bar: 50 μm.

(B) 2-P stimulation (indicated by red marker) of GCaMP6f/C1V1$_{T/T}$ co-expressing neurons at 1100 nm. GCaMP6f calcium transients of four co-expressing neurons of ten stimulation trials.

(C) Average fraction of responding cells at varying wavelengths at 80 mW.

(D) Average rate of evoked calcium transients at varying wavelengths at 80 mW (n = 27 neurons [10 trials each], 3 mice). One-way ANOVA nonparametric test, p = 0.68 (C), p = 0.74 (D).

(E) Average rate of evoked transients at stimulation wavelength of 1100 nm, at varying light intensities (40, 80, 120, and 210 mW). n = 26 neurons each, 3 mice. Unpaired t test, 40 mW vs 80 mW (p = 0.46), 40 mW vs 120 mW (p = 0.012), 40 mW vs 210 mW (p = 0.0039), 80 mW vs 120 mW (p = 0.012), 80 mW vs 210 mW (p < 0.0001), 120 mW vs 210 mW (p = 0.19).

Data are represented as mean ± SEM. Significance levels were *p < 0.05, **p < 0.01, ***p < 0.001 and ****p < 0.0001.

new techniques such as 3D-SHOT (Mardinly et al. 2018) are superior to scanning approaches as used in this study as they allow temporally uncoupled, parallel manipulation and imaging of a multitude of cells in three dimensions. However, holography-based systems are typically set at defined stimulation wavelengths as they are often used with fixed-wavelength ytterbium lasers, which do not allow for flexible exploration of spectral windows for effective and artifact-free optogenetic control. Therefore, a 2-P scanner-based solution as applied here might still be advantageous at least for methodological ground work in the field of all-optical physiology. It has to be noted that, in terms of light sources, novel designs providing two

independently tunable femtosecond-pulsed laser beams with extended wavelength spectrum could be introduced in a CGH-based setups as well, thereby increasing flexibility in contrast to fixed-wavelength lasers.

We commenced our framework with setting the specificity to detect underlying APs of our detection algorithm to 100% by correlating our optical data to the actual electrical activity of a neuron. This allowed us to completely avoid type I errors, i.e., mistaking movement- or stimulation light-induced artifacts with calcium transients devoid of an electrophysiological correlate and therefore contributing to false-positive detection of pathological activity patterns (e.g. early cortical hyperactivity) in a healthy brain. In our recent studies, we already applied a rigorous analysis routine to 2-P imaging data (Figure S4D). And indeed, this provided an improved platform for testing the efficacy of drug treatments (Arnoux et al., 2018; Ellwardt et al. 2018). Here, we extend this greatly conservative approach to all-optical physiology. Of course, this comes at cost of sensitivity of activity detection, especially low numbers of APs. It has to be noted that the initial proof-of-principle publications on new indicators, e.g., on GCaMP6f (Chen et al. 2013) do provide sensitivity but no specificity data. Certainly, also in our setup, we did identify calcium deflections upon single APs, but these could not be unambiguously separated from calcium deflections of non-physiological sources. Deconvolution-based algorithms, such as OASIS, may be superior in terms of sensitivity, and indeed, using this approach, the identification of single-AP-related calcium transients is feasible. Yet, it comes at a price of overall reduced specificity, particularly in noisy data (please see also (Stringer et al. 2019)). Conventional threshold-based algorithms, such as ours, might be advantageous particularly in cases, in which no ground truth detection exists. In addition, the specificity of these approaches is compromised by systematic artifacts induced by photostimulation. We here demonstrate that the amplitude of these artifacts can be in the range of the amplitude of calcium transients and define the spectral range for artifact-free all-optical experiments. On the basis of this finding, we cannot recommend automated analysis algorithms, which merely correlate normalized fluorescence values with other physiological parameters or the behavioral context and strongly suggest that a detection algorithm should be based on an event detection, i.e., the optical correlate of a neuronal action potential. Indeed, several elegant approaches take these characteristic dynamics into account, such as the peeling algorithm (Greenberg et al. 2014). But, ultimately, given the high variability of technical setups, expression levels and brain areas investigated, we still suggest employing single-cell electrophysiology to titrate each detection algorithm, as exemplified in this study. Of course, in 2-P all-optical experiments, these artifacts are less dramatic than in 1-P excitation (Schmid et al. 2016). However, also in 2-P excitation, these photostimulation artifacts still cause significant problems (Rickgauer et al. 2014; Carrillo-Reid et al. 2016; Forli et al. 2018; Mardinly et al. 2018; Chen et al. 2019; Marshel et al., 2019) and might resemble AP-related calcium transients (Carrillo-Reid et al. 2019), especially when high light intensities are applied. Up to now, this problem was addressed using three main approaches: (1) sacrificing pixels containing the artifact resulting in data loss (Chen et al. 2019; Marshel et al., 2019), (2) post hoc identification based on the temporal dynamics of the artifact in contrast to the AP-related transients (Rickgauer et al. 2014; Carrillo-Reid et al. 2016), which in our view is amenable only in data with highest signal-to-noise ratio, not reflecting the reality particularly in awake measurements, and (3) gating stimulation and recording lasers, reducing effective field of view (Mardinly et al. 2018). In contrast to the aforementioned studies, one study used a different configuration combining a blue-shifted opsin with a red-shifted indicator (Forli et al. 2018). However, also here, a photostimulation artifact was apparent, most likely due to the fact that the indicator was excited on his blue shoulder by the strong stimulation light and was dealt with by subtracting background or blanking a short period in the calcium trace (Forli et al. 2018). One further, major problem which cannot be addressed with any of these methods and is independent of the artifact amplitude is the following one: The photostimulation artifact will inevitably make it impossible to determine latencies of responses and will therefore hinder precise timing of evoked spikes as the exact onset of a transient will be hidden within the artifact.

Here, we provide evidence that at stimulation wavelengths of 1100 nm and above, stimulation artifacts range below noise level. This frees the researcher from the need for any post hoc and specificity-reducing methods of artifact minimization and opens up the use of higher stimulation light intensities, e.g., to overcome strong inhibitory tones, as reducing light intensities to minimize artifacts will necessarily reduce photocurrents (Rickgauer et al. 2014; Mardinly et al. 2018; Chen et al. 2019; Marshel et al., 2019). Indeed, increasing stimulation light intensities at the optimal stimulation wavelength 1100 nm significantly increased cellular response rates. And above all, stimulation at 1100 nm will still allow the exact determination of response latencies. On the aspect of spurious activation of the opsin by the light used for exciting the indicator: This type of cross talk is actually a far more significant problem for 1-P stimulation of opsins and indicators, i.e., 1-P all-optical physiology. We conducted a study on this earlier, finding a two-order-of

magnitude safety margin when using low yet efficient light intensities (Adelsberger et al. 2014). Efficient 2-P excitation of opsin is typically only effective at pixel dwell times of 6 μs and beyond, at least for the currently used opsins (Prakash et al. 2012). The current state of the art in 2-P calcium imaging uses resonant mirrors, yielding temporal resolutions of 30 Hz, and pixel dwell times of 1 μs or less, or inertia-free AOM (Acousto-optic modulator)-based systems with even higher frequencies and shorter pixel dwell times. Also, the wavelength used for excitation of GCaMP6f is well outside of the efficient excitation peak. And indeed, three recent studies did not find any significant spurious excitation of the opsin by the illumination light used for imaging, at least for light intensities of 40 mW and below. Mardinly and colleagues (Mardinly et al. 2018) explored the spurious activation of the newly designed soma-targeted opsin ST-ChroME while Ronzitti and colleagues (Ronzitti et al. 2017) used Chronos. We would like to emphasize that, Rickgauer et al. (Rickgauer et al. 2014) employed C1V1 as in this study and found that with an imaging power of 30–40 mW, this type of cross talk was negligible. Here, in our study we used even lower light intensities for imaging (10–30 mW).

All-optical physiology approaches using 2-P light sources for stimulation and imaging do not only face obstacles such as cross talk between indicator and opsin or limited efficacy of optogenetic stimulation, but the field needs to address putative heat-related side effects, which might impact neuronal physiology. This is particularly relevant for high stimulation laser powers, as used both in holographic and line-scanning-based 2-P optogenetic stimulation schemes. Chen et al. (Chen et al. 2019) and Mardinly et al. (Mardinly et al. 2018) conducted an assessment of heating-related artifacts in a CGH approach. In terms of line-scanning-based approaches, as conducted here, putative heat effects critically depend on the pixel dwell time, light power and wavelength. Earlier studies using wavelength of 920 nm, as employed for the excitation of the indicator, did not reveal effects on neuronal firing rate, confirmed by our own results here (Stujenske et al. 2015; Podgorski and Ranganathan 2016). Longer wavelengths as used for the stimulation of opsins should even reduce heat-related effects, at least only considering the effect of the wavelength (Stujenske et al. 2015; Podgorski and Ranganathan 2016). However, pixel dwell times in imaging schemes with resonant scanners range around 1 μs, while for optogenetics, pixel dwell times typically exceed 6 μs (Packer et al. 2015). Yet a designated study addressing heat-related effects using longer wavelength line scanning optogenetic schemes is clearly desirable.

Finally, we addressed an open question of the field in terms of the spectral efficacy of opsin activation beyond 1100 nm. As aforementioned, *in vitro* whole-cell electrophysiology measurements found an increase in photocurrents with increasing wavelengths up to 1040 nm (Prakash et al. 2012). Here, albeit only using C1V1 in *in vivo* 2-P calcium imaging experiments, we did not find a further significant increase in spectral efficacy beyond 1100 nm. However, this might be different for other 2-P excitable opsins.

The still new and evolving field of 2-P all-optical physiology opens up tremendous prospects (Iaccarino et al. 2018; Martorell et al. 2019), but we suggest a careful and holistic approach including a pipeline for further exploratory research as devised here in order to maximize translational power. In sum, for minimizing the artifact, stimulation wavelengths of 1100 nm and above are advisable, albeit beyond 1100 nm no further reduction became apparent. Efficacy for opsin stimulation did not exceed above 1100 nm, albeit a larger spectral separation could be beneficial, depending on the opsin-indicator pair used. For GCaMP6f, imaging wavelength of 920 nm seems to be optimal, combined with C1V1-based optogenetics at wavelength of 1100 nm, an efficacy beyond 70% is well achievable for light intensities between 150 and 200 mW. Note that all these parameters will critically depend on the imaging setup and also require tailored expression strategies, optimizing the entire pipeline (Stroh 2018).

Limitations of the study

In this study, we probed the indicator-opsin pair GCaMP6f/C1V1, as this combination seemed to be mostly used in the field (Rickgauer et al. 2014; Packer et al. 2015; Carrillo-Reid et al. 2016; Yang et al., 2018a; Zhang et al. 2018; Carrillo-Reid et al. 2019). However, the development of new opsin and indicator variants has advanced (Ronzitti et al. 2016; Mardinly et al. 2018; Chen et al. 2019; Marshel et al., 2019), and for newer opsin-indicator couples, different stimulation or imaging parameters might be optimal. Recent developments of new members of the family such as GCaMP7 or 8 might display even higher sensitivity toward single action potentials (Dana et al., 2019; Zhang et al., 2020), albeit as they are also based on the same or similar fluorophore, the same behavior concerning the wavelength dependency of the artifact can be expected. What is more, also somatic targeting of the opsin (Mardinly et al., 2018) might increase the efficacy of 2-P optogenetic stimulation, yet it will not change the wavelength dependency, provided the same opsin

is used. Furthermore, as mentioned above, our approach has important technical limitations compared to CGH-based all-optical experiments and is currently limited to one plane for imaging and stimulation.

METHODS

All methods can be found in the accompanying Transparent Methods supplemental file.

SUPPLEMENTAL INFORMATION

Supplemental Information can be found online at https://doi.org/10.1016/j.isci.2021.102184.

AUTHOR CONTRIBUTIONS

T.F., I.A., and J.D. are equally contributing first authors. A.S. designed the study. T.F. performed calcium imaging, all-optical experiments, and virus titration. I.A. and H.W. performed cell-attached recordings combined with calcium imaging and optogenetic stimulation. J.D. performed LFP experiments combined with optic fiber stimulations. T.F., I.A., J.D., H.B., and H.W. performed the imaging analysis. I.A. and J.D. performed the analysis of *in vivo* electrophysiology. J.D. performed confocal analysis. I.S. performed PSF measurements. A.S., J.D., T.F., I.A., H.W., and I. S. wrote the manuscript.

DECLARATION OF INTERESTS

I.S. is an employee of Light Conversion Ltd., the producer of one of the lasers used in this study.

REFERENCES

Adelsberger, H., Grienberger, C., Stroh, A., and Konnerth, A. (2014). In vivo calcium recordings and channelrhodopsin-2 activation through an optical fiber. Cold Spring Harb Protoc. *2014*, pdb prot084145.

Akerboom, J., Chen, T.W., Wardill, T.J., Tian, L., Marvin, J.S., Mutlu, S., Calderon, N.C., Esposti, F., Borghuis, B.G., Sun, X.R., et al. (2012). Optimization of a GCaMP calcium indicator for neural activity imaging. J. Neurosci. *32*, 13819–13840.

Arnoux, I., Willam, M., Griesche, N., Krummeich, J., Watari, H., Offermann, N., Weber, S., Narayan Dey, P., Chen, C., Monteiro, O., et al. (2018). Metformin reverses early cortical network dysfunction and behavior changes in Huntington's disease. Elife *7*, e38744.

Aschauer, D.F., Kreuz, S., and Rumpel, S. (2013). Analysis of transduction efficiency, tropism and axonal transport of AAV serotypes 1, 2, 5, 6, 8 and 9 in the mouse brain. PLoS One *8*, e76310.

Busche, M.A., Chen, X., Henning, H.A., Reichwald, J., Staufenbiel, M., Sakmann, B., and Konnerth, A. (2012). Critical role of soluble amyloid-beta for early hippocampal hyperactivity in a mouse model of Alzheimer's disease. Proc. Natl. Acad. Sci. U S A *109*, 8740–8745.

Carrillo-Reid, L., Han, S., Yang, W., Akrouh, A., and Yuste, R. (2019). Controlling visually guided behavior by holographic recalling of cortical ensembles. Cell *178*, 447–457.e5.

Carrillo-Reid, L., Yang, W., Bando, Y., Peterka, D.S., and Yuste, R. (2016). Imprinting and recalling cortical ensembles. Science 353, 691–694.

Chen, I.W., Ronzitti, E., Lee, B.R., Daigle, T.L., Dalkara, D., Zeng, H., Emiliani, V., and Papagiakoumou, E. (2019). In vivo submillisecond two-photon optogenetics with temporally focused patterned light. J. Neurosci. 39, 3484–3497.

Chen, T.W., Wardill, T.J., Sun, Y., Pulver, S.R., Renninger, S.L., Baohan, A., Schreiter, E.R., Kerr, R.A., Orger, M.B., Jayaraman, V., et al. (2013). Ultrasensitive fluorescent proteins for imaging neuronal activity. Nature 499, 295–300.

Dana, H., Sun, Y., Mohar, B., Hulse, B.K., Kerlin, A.M., Hasseman, J.P., Tsegaye, G., Tsang, A., Wong, A., Patel, R., et al. (2019). High-performance calcium sensors for imaging activity in neuronal populations and microcompartments. Nat. Methods 16, 649–657.

Dirnagl, U. (2016). Thomas Willis lecture: is translational stroke research broken, and if so, how can we fix it? Stroke 47, 2148–2153.

Dirnagl, U. (2019). Rethinking research reproducibility. EMBO J. 38, e101117.

Duda, G.N., Grainger, D.W., Frisk, M.L., Bruckner-Tuderman, L., Carr, A., Dirnagl, U., Einhaupl, K.M., Gottschalk, S., Gruskin, E., Huber, C., et al. (2014). Changing the mindset in life sciences toward translation: a consensus. Sci. Transl. Med. 6, 264cm212.

Ellwardt, E., Pramanik, G., Luchtman, D., Novkovic, T., Jubal, E.R., Vogt, J., Arnoux, I., Vogelaar, C.F., Mandal, S., Schmalz, M., et al. (2018). Maladaptive cortical hyperactivity upon recovery from experimental autoimmune encephalomyelitis. Nat. Neurosci. 21, 1392–1403.

Emiliani, V., Cohen, A.E., Deisseroth, K., and Hausser, M. (2015). All-optical interrogation of neural circuits. J. Neurosci. 35, 13917–13926.

Fois, C., Prouvot, P.H., and Stroh, A. (2014). A roadmap to applying optogenetics in neuroscience. Methods Mol. Biol. 1148, 129–147.

Forli, A., Vecchia, D., Binini, N., Succol, F., Bovetti, S., Moretti, C., Nespoli, F., Mahn, M., Baker, C.A., Bolton, M.M., et al. (2018). Two-photon bidirectional control and imaging of neuronal excitability with high spatial resolution in vivo. Cell Rep. 22, 3087–3098.

Greenberg, D.S., Wallace, D.J., and Kerr, J.N. (2014). Imaging neuronal population activity in awake and anesthetized rodents. Cold Spring Harb. Protoc. 2014, 912–922.

Grienberger, C., and Konnerth, A. (2012). Imaging calcium in neurons. Neuron 73, 862–885.

Iaccarino, H.F., Singer, A.C., Martorell, A.J., Rudenko, A., Gao, F., Gillingham, T.Z., Mathys, H., Seo, J., Kritskiy, O., Abdurrob, F., et al. (2018). Author Correction: gamma frequency entrainment attenuates amyloid load and modifies microglia. Nature 562, E1.

Mardinly, A.R., Oldenburg, I.A., Pegard, N.C., Sridharan, S., Lyall, E.H., Chesnov, K., Brohawn, S.G., Waller, L., and Adesnik, H. (2018). Precise multimodal optical control of neural ensemble activity. Nat. Neurosci. 21, 881–893.

Marshel, J.H., Kim, Y.S., Machado, T.A., Quirin, S., Benson, B., Kadmon, J., Raja, C., Chibukhchyan, A., Ramakrishnan, C., Inoue, M., et al. (2019). Cortical layer-specific critical dynamics triggering perception. Science 365, eaaw5202.

Martorell, A.J., Paulson, A.L., Suk, H.J., Abdurrob, F., Drummond, G.T., Guan, W., Young, J.Z., Kim, D.N., Kritskiy, O., Barker, S.J., et al. (2019). Multi-sensory gamma stimulation ameliorates Alzheimer's-associated pathology and improves cognition. Cell 177, 256–271 e222.

Packer, A.M., Peterka, D.S., Hirtz, J.J., Prakash, R., Deisseroth, K., and Yuste, R. (2012). Two-photon optogenetics of dendritic spines and neural circuits. Nat. Methods 9, 1202–1205.

Packer, A.M., Russell, L.E., Dalgleish, H.W., and Hausser, M. (2015). Simultaneous all-optical manipulation and recording of neural circuit activity with cellular resolution in vivo. Nat. Methods 12, 140–146.

Piper, S.K., Grittner, U., Rex, A., Riedel, N., Fischer, F., Nadon, R., Siegerink, B., and Dirnagl, U. (2019). Exact replication: foundation of science or game of chance? PLoS Biol. 17, e3000188.

Podgorski, K., and Ranganathan, G. (2016). Brain heating induced by near-infrared lasers during multiphoton microscopy. J. Neurophysiol. 116, 1012–1023.

Prakash, R., Yizhar, O., Grewe, B., Ramakrishnan, C., Wang, N., Goshen, I., Packer, A.M., Peterka, D.S., Yuste, R., Schnitzer, M.J., and Deisseroth, K. (2012). Two-photon optogenetic toolbox for fast inhibition, excitation and bistable modulation. Nat. Methods 9, 1171–1179.

Rickgauer, J.P., Deisseroth, K., and Tank, D.W. (2014). Simultaneous cellular-resolution optical perturbation and imaging of place cell firing fields. Nat. Neurosci. 17, 1816–1824.

Rochefort, N.L., Garaschuk, O., Milos, R.I., Narushima, M., Marandi, N., Pichler, B., Kovalchuk, Y., and Konnerth, A. (2009). Sparsification of neuronal activity in the visual cortex at eye-opening. Proc. Natl. Acad. Sci. U S A 106, 15049–15054.

Ronzitti, E., Conti, R., Papagiakoumou, E., Tanese, D., Zampini, V., Chaigneau, E., Foust, A.J., Klapoetke, N.C., Boyden, E.S., and Emiliani, V. (2016). Sub-millisecond optogenetic control of neuronal firing with two-photon holographic photoactivation of Chronos. bioRxiv 37, 10679–10689.

Ronzitti, E., Conti, R., Zampini, V., Tanese, D., Foust, A.J., Klapoetke, N., Boyden, E.S., Papagiakoumou, E., and Emiliani, V. (2017). Submillisecond optogenetic control of neuronal firing with two-photon holographic photoactivation of chronos. J. Neurosci. 37, 10679–10689.

Schmid, F., Wachsmuth, L., Schwalm, M., Prouvot, P.H., Jubal, E.R., Fois, C., Pramanik, G., Zimmer, C., Faber, C., and Stroh, A. (2016). Assessing sensory versus optogenetic network activation by combining (o)fMRI with optical Ca2+ recordings. J. Cereb. Blood Flow Metab. 36, 1885–1900.

Schwalm, M., Schmid, F., Wachsmuth, L., Backhaus, H., Kronfeld, A., Aedo Jury, F., Prouvot, P.H., Fois, C., Albers, F., van Alst, T., et al. (2017). Cortex-wide BOLD fMRI activity reflects locally-recorded slow oscillation-associated calcium waves. Elife 6, e27602.

Stosiek, C., Garaschuk, O., Holthoff, K., and Konnerth, A. (2003). In vivo two-photon calcium imaging of neuronal networks. Proc. Natl. Acad. Sci. U S A 100, 7319–7324.

Stringer, C., Pachitariu, M., Steinmetz, N., Reddy, C.B., Carandini, M., and Harris, K.D. (2019). Spontaneous behaviors drive multidimensional, brainwide activity. Science 364, 255.

Stroh, A. (2018). Optogenetics: A Roadmap (Humana Press).

Stroh, A., Adelsberger, H., Groh, A., Ruhlmann, C., Fischer, S., Schierloh, A., Deisseroth, K., and Konnerth, A. (2013). Making waves: initiation and propagation of corticothalamic Ca2+ waves in vivo. Neuron 77, 1136–1150.

Stujenske, J.M., Spellman, T., and Gordon, J.A. (2015). Modeling the spatiotemporal dynamics of light and heat propagation for in vivo optogenetics. Cell Rep. 12, 525–534.

Yang, J.W., Prouvot, P.H., Reyes-Puerta, V., Stuttgen, M.C., Stroh, A., and Luhmann, H.J. (2017). Optogenetic modulation of a minor fraction of parvalbumin-positive interneurons specifically affects spatiotemporal dynamics of spontaneous and sensory-evoked activity in mouse somatosensory cortex in vivo. Cereb. Cortex 27, 5784–5803.

Yang, W., Carrillo-Reid, L., Bando, Y., Peterka, D.S., and Yuste, R. (2018a). Simultaneous two-photon imaging and two-photon optogenetics of cortical circuits in three dimensions. Elife 7, e32671.

Yang, J.-W., Prouvot, P.-H., Stroh, A., and Luhmann, H.J. (2018b). Combining optogenetics with MEA, depth-resolved LFPs and assessing the scope of optogenetic network modulation. Neuromethods 133, 133–152, SpringerNature (Optogenetics: A Roadmap).

Zhang, Y., M. Rózsa, D. Bushey, J. Zheng, D. Reep, G.J. Broussard, A. Tsang, G. Tsegaye, R. Patel, S. Narayan, et al (2020). jGCaMP8 fast genetically encoded calcium indicators. https://doi.org/10.25378/janelia.13148243.

Zhang, Z., Russell, L.E., Packer, A.M., Gauld, O.M., and Hausser, M. (2018). Closed-loop all-optical interrogation of neural circuits in vivo. Nat. Methods 15, 1037–1040.

Supplemental information

Exploring two-photon optogenetics

beyond 1100 nm for specific

and effective all-optical physiology

Ting Fu, Isabelle Arnoux, Jan Döring, Hendrik Backhaus, Hirofumi Watari, Ignas Stasevicius, Wei Fan, and Albrecht Stroh

Supplementary Information

Supplementary Figure legends:

Fig. S 1. Functional calcium transients can only be detected in a rather narrow spectral window: **A** Sensitivity / Specificity plot employing OASIS deconvolution toolbox. Setting the limit of the peak detection to 100 % of the estimated noise band results in a mean sensitivity of 91 % ± 12 % at a specificity of 15 % ± 9 %. Increasing limits to 300, 500, 700 and 1000 % of the noise band reduces the sensitivity to 84 % ± 13 %, 72 % ± 14 %, 63 % ± 18 %, and 53 % ± 21 % while the specificity increases to 30 % ± 9 %, 48 % ± 16 %, 54 % ± 18 %, and 67 % ± 25 %. **B** 2-P imaging of GCaMP6f expressing neurons at four different Ti:Sa wavelengths (860, 880, 900, 920 nm) in layer II/III of mouse visual cortex *in vivo*. The same three neurons (white circles) are depicted at each wavelength. Scale bar: 50 μm. **C** Corresponding calcium traces of depicted neurons. **D** Normalized number of active cells at different wavelengths. **E** Normalized number of calcium transients at each wavelength. **F** Average transient frequencies at different wavelengths. Mann-Whitney-Test, 860 nm vs. 880 nm p = 0.0026, 860 nm vs 900 nm p = 0.0003, 860 nm vs 920 nm, p = 0.0001, 880 nm vs. 900 nm p = 0.51, 880 nm vs 920 nm p = 0.28, 900 nm vs 920 nm p = 0.38, n = 66 cells, 2 mice.

Fig. S 2. Technical concepts for achieving extended-wavelength-spectrum 2-P all-optical interrogations and determining the spatial specificity of 2-P optogenetic stimulation. A Microscope set up based on one Ti:Sa laser used for both pumping the OPO and for GCaMP6f imaging by employing a beam splitter. The OPO delivers a broader wavelength range for excitation (1100 - 1400 nm). The imaging wavelength is guided to a resonant scanner for full-field imaging of GCaMP6f at 920 nm and the stimulation wavelength is guided to a temporally uncoupled galvo scanner for independent optogenetic control. PMT = Photomultiplier Tube,

BS = Beamsplitter. **B** Employing wo independent Ti:Sa lasers, one is dedicated to GCaMP6f-imaging and the other is pumping the OPO. **C** A dual color laser is delivering two independently tunable laser beams. Imaging wavelengths (680 - 960 nm) are guided to a resonant scanner and stimulation wavelengths (950 - 1300 nm) are guided to a separate galvo scanner. **D** Fluorescent nanobeads, 2-P horizontal (XY) and vertical (YZ) cross sections at 920 nm. **E** X axis single bead fluorescent signal and gaussian fit for point spread function (PSF) and full width half maximum (FWHM) measurements. **F** PSF measurements in X, Y and Z direction for varying excitation wavelengths. Error margins are extracted from n = 5 average beads' measurements for each tested wavelength.

Fig. S 3. Probing functional expression of actuator and indicator by applying 1-P and 2-P optogenetic stimulation by using optimized titers of AAVs achieving strong co-expression. A-C Titration of AAVs encoding for indicator and opsin proteins: confocal micrographs of different titer combinations (GCaMP6f (green) / C1V1$_{T/T}$ (red): [0.62 * 10^{10} / ml] / [6.66 * 10^{11} / ml], [0.92 * 10^{10} / ml] / [3.33 * 10^{11} / ml] and [1.84 * 10^{10} / ml] / [3.33 * 10^{11} / ml], scale bar 75 μm). Left column: green channel at 488 nm. Middle column: red channel at 584 nm. Right column: overlay. **(C)** is identical to Fig. 4 A. **D** Density of C1V1$_{T/T}$ expressing cells in different cortical layers of primary visual cortex. Unpaired t-test, layer II/III vs layer V/VI p < 0.0001, Mann-Whitney test layer II/III vs layer IV p = 0.15, layer IV vs layer V/VI p = 0.0079. **E** Density of C1V1$_{T/T}$ / GCaMP6f co-expressing cells in different cortical layers of V1. Unpaired t-test layer II/III vs layer V/VI p = 0.021, Mann-Whitney test layer II/III vs layer IV p = 0.016, layer IV vs layer V/VI p = 0.0079. **F** Relative fraction of co-expressing cells in different cortical layers of V1. Unpaired t-test layer II/III vs layer V/VI p = 0.0014, Mann-Whitney test layer II/III vs layer IV p = 0.11 , layer IV vs layer V/VI p = 0.11 . D-F n = 175 cells, 5 brain slices (70 μm), 3 mice. **G** *In vivo* 2-P image of shadow-patched C1V1-EYFP-expressing

(green) neuron in layer II/III of mouse visual cortex and OPO-based 2-P stimulation using raster scan patterns at 1100 nm. Stimulation was delivered every 10 s and was defined by a duration of 68 ms, a pixel dwell time of 6 μs, a line scan resolution of 0.5 μm and a laser intensity of 37 mW. Patch pipette filled with AlexaFluo594 (red). Scale bar: 15 μm. **H, I** Combined LFP and juxtacellular recordings revealed LFP responses upon 1-P stimulations at 552 nm (**H**) and 2-P stimulation at 1100 nm (**I**), respectively. **J** Average latencies upon 2-P raster scan stimulations at different light intensities. Unpaired t-test, 14 mW vs 37 mW $p = 0.0001$, 14 mW vs 58 mW $p < 0.0001$, 37 mW vs 58 mW $p < 0.0001$, n = 26 responses, 1 neuron. **K** Average number of events triggered by 2-P raster scan stimulations at different light intensities. Mann-Whitney test, 14 mW vs 37 mW $p = 0.06$, 14 mW vs 58 mW $p < 0.0001$, 37 mW vs 58 mW $p < 0.0001$, n = 26 responses, 1 neuron. **L** Average photocurrents, 14 mW vs 37 mW $p < 0.0001$, 14 mW vs 58 mW $p < 0.0001$, 37 mW vs 58 mW $p < 0.0001$, n = 26 responses, 1 neuron. **M** Response probabilities, n = 26 responses, 1 neuron.

Fig. S 4. Brain-state informed 2-P all-optical physiology at 1100 nm and 80 mW light intensity. A Typical field of view during 2-P calcium recording of the same cortical microcircuit in layer II/III of mouse visual cortex during different brain states (left). Scale bar: 50 μm. **B** Corresponding calcium traces devised from the entire area of GCaMP6f-expression integrating cellular and neuropil signals. Different brain states are defined by their distinct patterns of spontaneous neural activity and can be induced by varying levels of anesthesia. Light isoflurane anesthesia leads to an activated or persistent state where spontaneous activity is defined by fast low-amplitude oscillations (upper), while deep anesthesia leads to slow oscillations characterized by spontaneous fluctuations between intermittent depolarized Up states and hyperpolarized Down states (lower). **C** Representative calcium traces of five co-expressing neurons (n = 27

neurons, 10 trials each, 3 mice). 2-P stimulation was indicated by yellow line, identified responses colored in red. **D** 2-P calcium imaging analysis pipeline. Recording of GCaMP6f calcium imaging was motion corrected (I) and visible neurons were semi-manually selected with a custom written Matlab code (II). Intensity traces were extracted by averaging all pixel values within each identified neuron, resulting in an intensity time course for each neuron (III). Calcium transients were detected by applying a standard deviation threshold-based algorithm and a binarized train was generated where calcium transients are represented as 1 and periods of quiescence are represented as 0 (IV). Statistical tests can be applied to the binarized trains for further investigations (V).
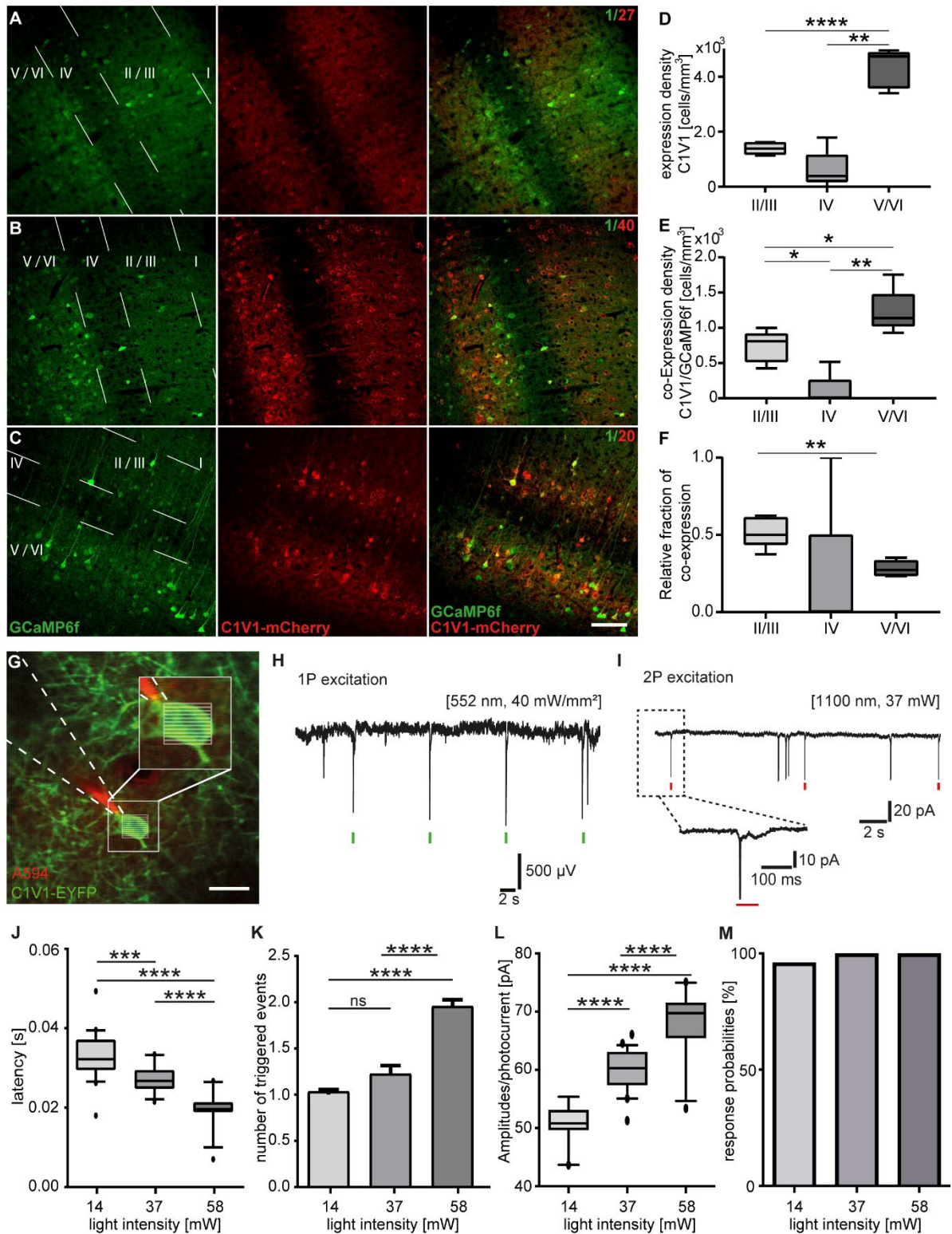
Supplementary Figures

Supplementary Figure 1 Functional calcium transients can only be detected in a rather narrow spectral window. Related to Figure 1
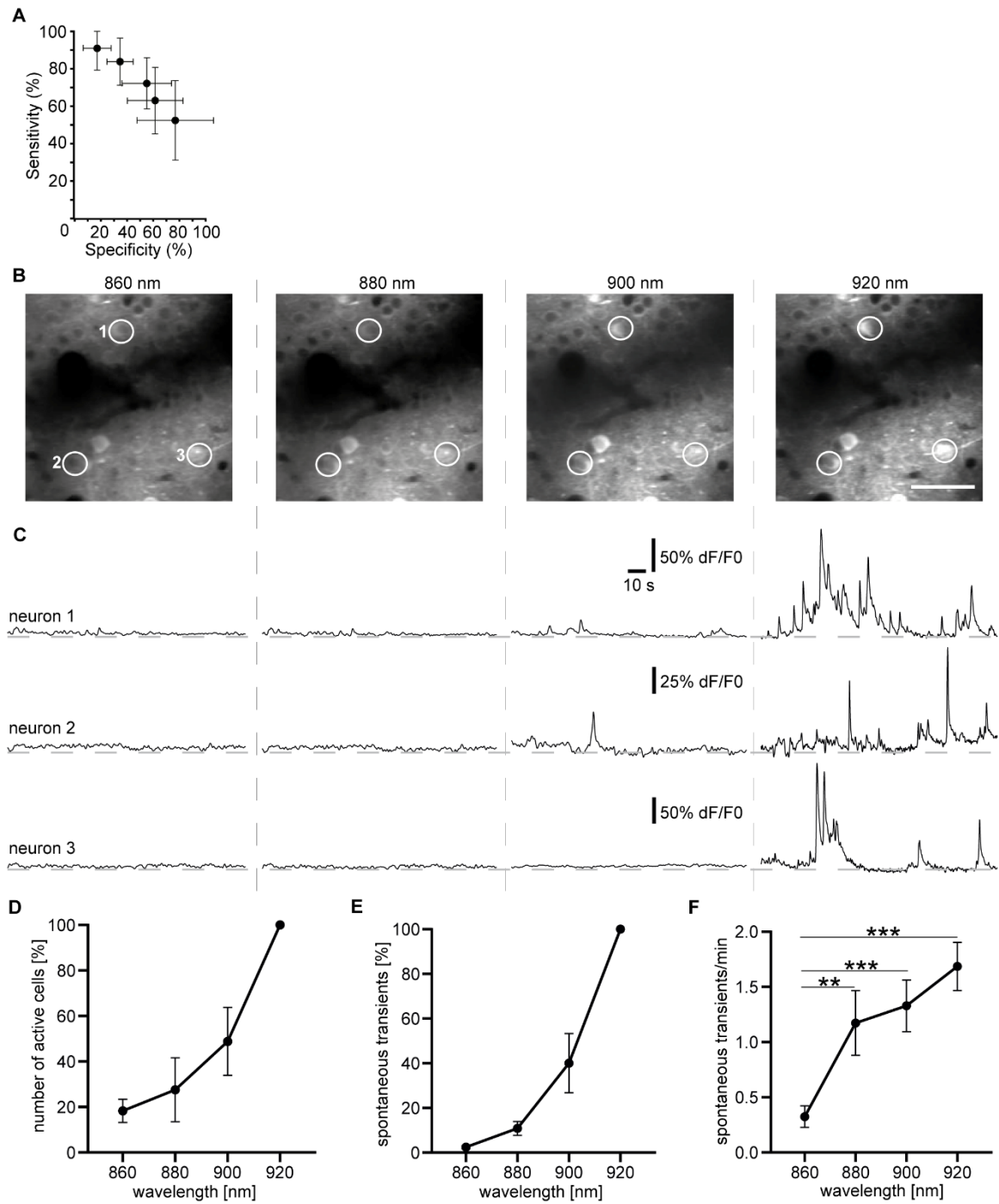
Supplementary Figure 2 Technical concepts for achieving extended-wavelength-spectrum 2-P all-optical interro-gations and determining the spatial specificity of 2-P optogenetic stimulation. Related to Figure 2
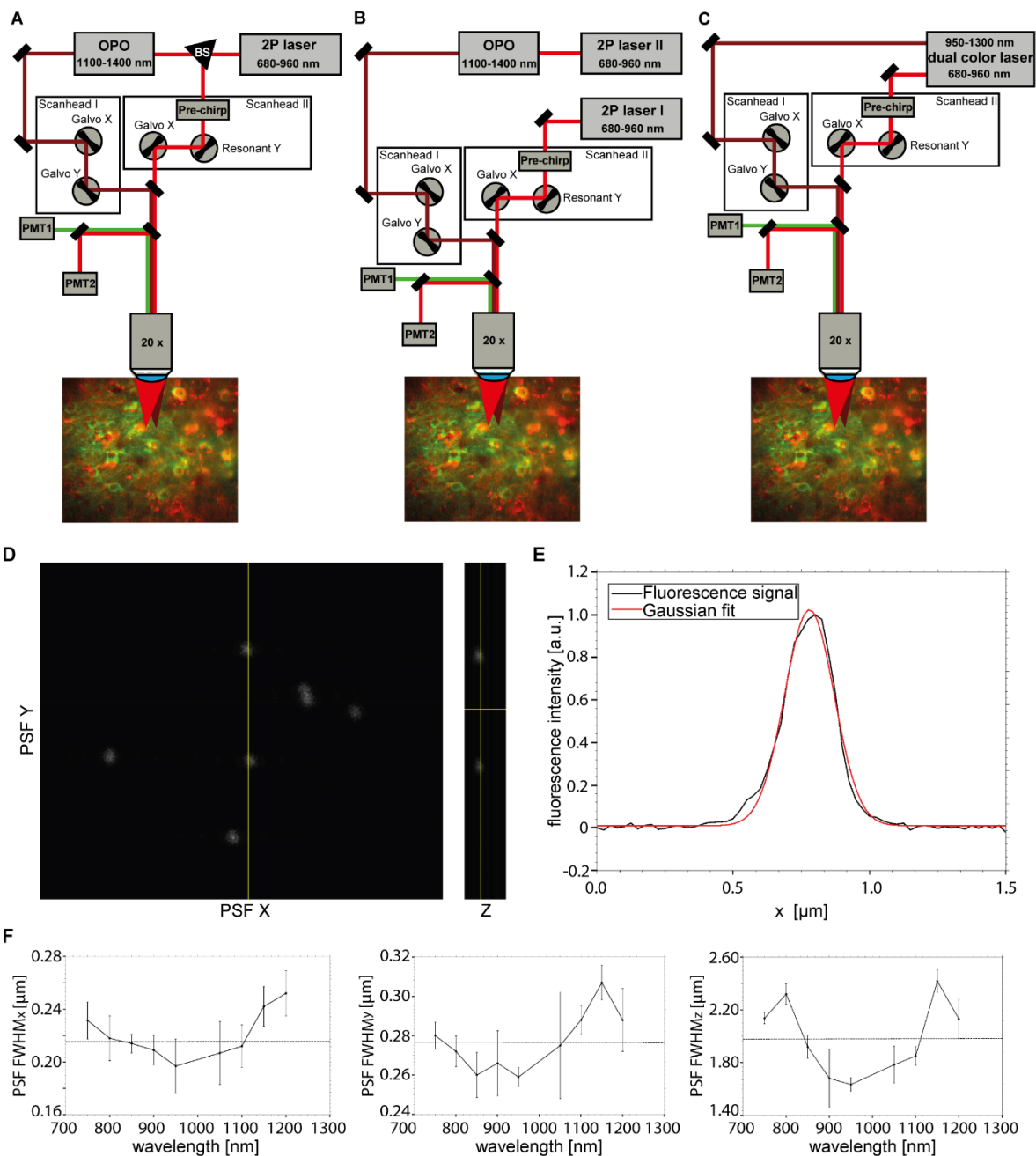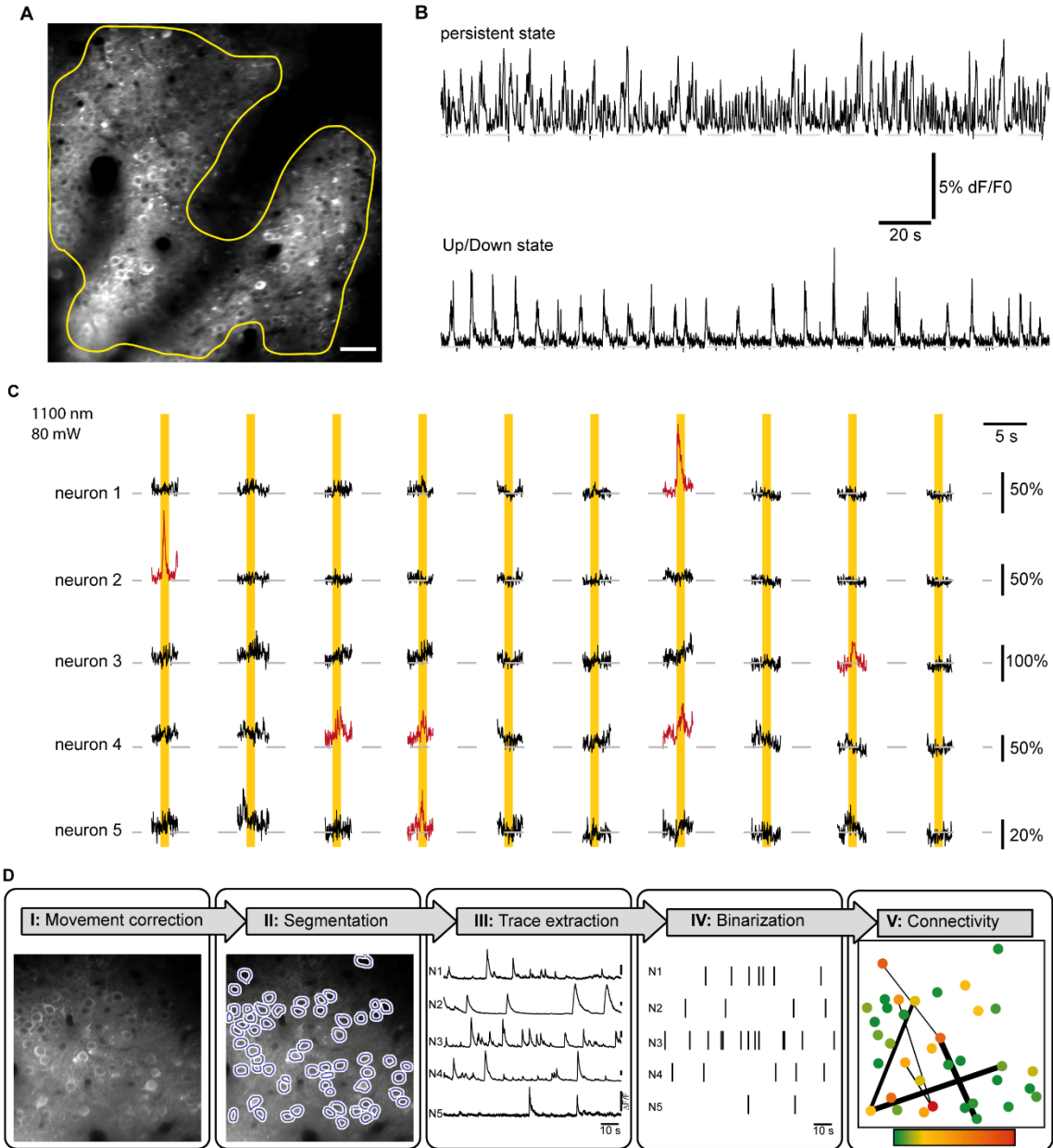
Supplementary Figure 3 Probing functional expression of actuator and indicator by applying 1-P and 2-P opto-genetic stimulation by using optimized titers of AAVs achieving strong co-expression. Related to Figure 2, 3

Supplementary Figure 4 Brain-state informed 2-P all-optical physiology at 1100 nm and 80 mW light intensity. Related to Figure 4

Transparent Methods

Study design. The overarching research goal was to improve all-optical approaches for their use in translational models of neurological disorders. Here we pursued three a priori defined research objectives: (I.) Achieving utmost specificity in terms of the detection of AP-related calcium transients, (II.) investigating the currently maximally achievable spectral range for all-optical experiments concerning, both, imaging and stimulation and to determine the interference of photostimulation artifacts, and (III.) probing the wavelength dependency of effective optogenetic control. The study is an explorative study on non-randomized female and male C57/BL6 mice co-expressing C1V1 and GCaMP6f in cortical neurons. It represents a completely new experimental paradigm with designated hardware components, which has not been used in this field of research, yet. Key designated components of this study are a state-of-the-art 2-P microscope integrated with an OPO or a Cronus laser, C1V1 as optogenetic actuator and GCaMP6f as calcium indicator. Particularly in experiments exploring the three a priori defined research objectives (Fig. 1, Fig. 3 and Fig. 4) sample sizes were determined by power analysis using the effect size and accuracy from our earlier studies. Light power levels for optogenetic stimulation were based on previous studies *(Prakash, Yizhar et al. 2012, Packer, Russell et al. 2015)*.

Animals. All experiments were carried out along institutional animal welfare guidelines and approved by the Landesuntersuchungsamt Koblenz, State of Rhineland-Palantine, Germany. For experiments adult female and male C57/BL6 mice were used.

Stereotactic virus injections and chronic window preparations. For 2-P all-optical experiments GCaMP6f was co-expressed with the opsin $C1V1_{T/T}$. This was achieved by titration of both viral solutions. Stock solutions of AAV1.Syn.Flex.GCaMP6f-WPRE.SV40 (3.67×10^{11} /

mL, Penn Vector Core, University of Pennsylvania, PA, USA) and rAAV2/CamKIIa-C1V1(E122T/E162T)-TS-mCherry (1.0×10^{12} / ml, UNC Vector Core, NC, USA) were prepared by diluting with PBS and stored at 4 °C. Different titers were tested ($[0.62 \times 10^{10}$ / ml] / $[6.66 \times 10^{11}$ / ml], $[0.92 \times 10^{10}$ / ml] / $[3.33 \times 10^{11}$ / ml] and $[1.84 \times 10^{10}$ / ml] / $[3.33 \times 10^{11}$ / ml]). For LFP experiments rAAV2/Ef1a-DIO-C1V1(E122T/E162T)-TS-mCherry (UNC Vector Core, NC, USA) was injected alongside with rAAV2/PKG-Cre (UNC Vector Core, NC, USA) in a ratio of $[1.44 \times 10^{13}$ / ml] / $[4.0 \times 10^{12}$ / ml]. Adult C57/BL6 mice anesthetized with isoflurane in O_2 (Abbvie, Ludwigshafen, Deutschland) were placed in a stereotactic frame (Kopf, CA, USA) and warmed with a heating pad (World Precision Instruments, Sarasota, FL, USA). For virus injections, a craniotomy was carried out above V1 with 3.0 mm posterior to Bregma and 2.5 mm lateral to the midline. Viral constructs were delivered though a small durotomy by a glass pipette (Hirschmann Laborgeräte, Eberstadt, Germany) via a custom-made loading system including a syringe and a plastic tubing using manual pressure. The pipette was slowly inserted and approximately 300 nl of the viral solution was injected with an injection-speed of 0.1 µl / min *(Cardin, Carlen et al. 2009)* at a depth of 200 µm targeting layer II/III and 600 µm targeting layer V/VI. Before retraction, the pipette remained in place for 5 minutes preventing an outward flow of the viral solution. For chronic window preparations, the skull was exposed to fix the head-holder on the mouse's head. Using the identical stereotactic coordinates as for histology a circular cranial window was prepared above V1. The virus injection procedure was conducted as described above. After the injection of the viral constructs, the opening was closed with a circular cover slip (Electron Microscopy Sciences, Hatfield, PA, USA) at a diameter of 4 mm.

Histology, confocal imaging and quantification of co-expression. For characterization of co-expression, animals were perfused trancardially with 4 % PFA 5 weeks post injection.

Brains were postfixed in 4 % PFA for 24 hours until they were sliced (70 µm thickness) using a Leica Vibratome (Leica, Wetzlar, Germany). Slices were directly mounted on an object slide (Gerhard Menzel, Braunschweig, Germany) with Vectashield Mounting Medium (Vector Laboratories, Burlingame, CA, USA) and fixed with a cover slip (Gerhard Menzel). Brain tissue sections were analyzed with a Leica SP8 confocal microscope (Leica) equipped with a Leica 20 x HCX PL APO dry (NA = 0.75) objective. To determine the density of $C1V1_{T/T}$ expressing and $C1V1_{T/T}$ / GCaMP6f co-expressing cells in V1, all cells with smooth and strong expression within the volume of strong homogeneous fluorescence were counted separately for each layer by using the cell counter plug-in of ImageJ (https://imagej.nih.gov/ij/). The density of cells per mm^3 in cortical layers II/III, IV, V/VI was calculated by dividing the total number of cells within the volume of strong homogenous fluorescence in each layer by the volume. Expression densities and fraction of expressing cells of all counted slices were averaged for each layer by calculating arithmetic means.

In vivo **electrophysiology.** For LFP recordings mice were injected with rAAV2/Efla-DIO-C1V1-(E122T/E162T)-TS-mCherry + rAAV2/PKG-Cre as described above. General anesthesia was performed with an intraperitoneal injection of 2.5 µl / g containing 0.5 µl Medetomidin (Pfizer AG, New York, USA; 1 mg / ml), 1 µl Midazolam (Roche Pharma AG, Basel, Switzerland; 5 mg / ml) and 1 µl Fentanyl (Sintetica S.A., Mendrisio, Switzerland; 50 µg / ml). The coordinates of preceding virus injection were set and an acute 2 x 2 mm cranial window was prepared using a dental drill. With a fluorescence lamp, the localization of the virus expressing cortical area was determined. For LFP recordings patch-pipettes (1.5 - 3 MΩ) were filled with PBS and inserted into the brain tissue close to the virus expressing region in a depth of - 300 µm. The LFP signals were recorded with an EXT-02F/2 amplifier (npi Electronic, Tamm, Ger-

many). The signal was filtered low pass at 300 Hz without high pass filter. Optogenetic stimulation was delivered by a 20 mW solid-state laser at 552 nm coupled with an acoustic-optic modulator (Crystal Technology, Palo Alto, CA) for rapid control of laser intensity. The laser beam was bundled into an optic multimode fiber (Thorlabs, Grünberg, Germany) using a fiber collimator (Thorlabs). The fiber had an outer diameter of 0.2 mm, a core diameter of 0.1 mm and a NA of 0.48. The fiber was guided along the arm of the stereotactic setup and placed above the virus expressing region in physical contact with the intact dura mater. Single 10 ms stimuli were applied with approximately 60 mW / mm^2 light density. The voltage signals were collected with an analog-digital converter (CED, Cambridge, UK), displayed in real-time and saved with the appertaining software Spike 2 (CED, Cambridge, UK) on a computer (Dell Inc., Round Rock, TX, USA). The data was collected with a recording frequency of 1 kHz. Amplitudes were analyzed with Igor Pro (WaveMetrics, Portland, OR, USA) and quantified with GraphPad (GraphPad Software Inc., La Jolla, CA, USA). Average response amplitudes were calculated by using the arithmetic mean.

For juxtacellular recordings mice were injected with AAV1-Syn-GCaMP6f-WPRE-SV40, AAV2-CaMKIIa-C1V1(E122T/E162T)-TS-mCherry or AAV2-CaMKIIa-C1V1(E122T/E162T)-TS-EYFP. Three weeks later, the mouse was anesthetized with isoflurane and an acute craniotomy above V1 was prepared as described above. The exposed cortex was superfused with warm PBS. To dampen heartbeat- and breathing-induced motion, the cranial window was filled with 1 % agarose. Juxtacellular recordings were made by visually targeting GCaMP6f- or C1V1-expressing cells under 2-P vision in layer II/III of V1. Patch electrodes (4 – 6 MΩ) were filled (in mM): 10 HEPES, 1 MgCl$_2$, 2 CaCl$_2$, 150 NaCl, 2.5 KCl, 20 glucose and 10 Alexa Fluor 594 or Alexa Fluro 488 for pipette visualization. Signals were recorded with an ELC-03XS amplifier (npi Electronic, Tamm, Germany). Squarish ROIs (~ 30 x 30 μm) were placed onto the C1V1-expressing cells and raster scanning was performed.

Stimulation was delivered every 10 s and was defined by a duration of 68 ms, a pixel dwell time of 6 μs and a line scan resolution of 0.5 μm. The maximum laser intensity applied was 147 mW at 1100 nm. The voltage signals were collected and analyzed as described above and analyzed with a 250 ms binning window.

2-P calcium imaging and 2-P optogenetic stimulations. Chronic imaging experiments were performed earliest four weeks post injection to ensure sufficient co-expression of GCaMP6f and C1V1$_{T/T}$. For imaging animals were anesthetized with isoflurane and fixed on a custom-made table. An isoflurane dose of 1.0 - 1.5 % isoflurane / O_2 resulted in an average breathing rate of 50 - 70 bpm and reliably induced slow-oscillatory state with its characteristic Up/Down state transitions. An anesthesia dose of 0.6 - 1.0 % lead to recordings in persistent state. Here the breathing rate of the animal was 100 - 110 bpm. The custom-made 2-P microscope set-up (LaVision Biotec, Bielefeld, Germany) was equipped with a resonant scanner for fast full-field scanning up to 35 Hz. A mode-locked femtosecond-pulsed Tisa:Sapphire laser (Coherent, CA, USA) was used at 860, 880, 900 and 920 nm for imaging GCaMP6f expressing cells. The laser operated with 1-20 % of its maximal power output (3 W). The imaging plane was usually between 250 ± 100 μm below the cortical surface and the field of view was 466 x 466 μm using a Zeiss W-Plan-Apochromatic 20 x DIC VIS-IR objective (NA = 1.0). For all-optical experiments with GCaMP6f / C1V1$_{T/T}$ two different technical approaches were used. In the first implementation, the imaging was performed with the aforementioned Ti:Sapphire laser and the 2-P excitation of C1V1$_{T/T}$ was conducted with an optical parametric oscillator (Coherent, CA, USA) delivering light between with (1100 - 1400 nm) and pumped by a second independent Ti:Sa laser. Alternatively, both imaging and excitation were performed with a single femtosecond laser with two independently tunable output channels (Light Conversion Ltd., Vilnius, Lithuania). The first tunable channel (680 - 960 nm) was used for 2-P imaging, the second

tunable channel (950 - 1300 nm) was used for 2-P excitation of $C1V1_{T/T}$. The laser operated with 1-30 % of its maximal output power (1.2 W) in the imaging channel and 1-50 % of its maximal output power in the excitation channel (1.1 W). The pulse durations of both channels were 130 ± 20 fs across the wavelength tuning ranges, provided by manufacturer. The pulses were synchronous with repetition rate of 76 MHz each. In both cases only the 2-P beam used for imaging was coupled to the fast resonant scanner and the second longer wavelength was coupled to the additional galvanometric-scanner. Laser intensity was controlled by an electro-optical modulator (Coherent, CA, USA). Two 1-P lasers at 488 and 561 nm (High Performance OBIS$_{TM}$ Laser Systems, Coherent, Santa Clara, CA) were also coupled to the additional galvanometric scanner. For signal collection a high sensitive PMT (Hamamatsu, Hamamatsu, Japan) was used. Multiple $C1V1_{T/T}$ expressing neurons were stimulated individually or in full-field manner. Using ROI-based stimulation up to 6 ROIs were placed onto the cells of interest and raster scanning of each ROI was performed. Stimulation was delivered every 10 s and was defined by a pixel dwell time of 6 µs and a line scan resolution of 0.5 - 2 µm. The maximum laser intensity applied was 210 mW at 1100 nm. The nanobead sample (Invitrogen, Carlsbad, CA, USA) was used to measure point spread functions across wavelength tuning ranges for imaging and excitation. Images of fluorescent nanobeads and FWHM values were extracted in all three dimensions and fitted using a gaussian distribution.

2-P calcium imaging data analysis. The analysis of 2-P calcium imaging data follows a pipeline concept (Fig. S 8). Firstly, the calcium imaging data was acquired with Imspector (LaVision Biotec, Bielefeld, Germany). Afterwards image series were imported into MatLab (The MathWorks, Natick, MA, USA) and run through a custom semi-automated algorithm. In a first step, the algorithm created an average image of the image series. On this average image individual neurons were manually depicted as ROIs. For every ROI at any given time point an

average value of fluorescence intensity was determined by averaging the fluorescence values of each pixel within the ROI in every single image of the series, resulting in a calcium trace for every ROI. A baseline region was selected in every trace and measured fluorescence levels of each ROI were converted into relative changes in fluorescence (dF / F_0) in relation to the selected baseline region. In the next step, the data was transferred to Igor Pro and calcium analysis was conducted with a custom-made program suite. Transients were detected by a peak detection algorithm already used in a previous study by ours *(Arnoux, Willam et al. 2018)*. This algorithm auto-detected calcium transients wherever the amplitude of the calcium signal exceeded 3 - 3.5 SD above the mean, the first derivative crossed zero and the second derivative was negative. 100 % specificity was achieved by increasing this threshold and by calibrating the algorithm using simultaneous juxtacellular recordings. The program suite also enclosed a tool modeling the decay of the calcium deflection and categorizing for exponential and non-exponential decays, therefore taking into account a typical feature of the shape of an AP-related calcium transient. In this tool the decay was fitted by Igor Pro's built-in curve fitting feature CurveFit, which fits a single exponential curve between the peak and the tail of an autodetected transient. Specificity and sensitivity were confirmed using parallel *in vivo* 2-P GCaMP6f imaging and juxtacellular recordings as described above. The traces were pre-treated by binomial (Gaussian) smoothing 30 - 40 times, followed by a high-pass filter with the end of the reject band at 0.1 / Fs, the start of the pass band at 0.12 / Fs, the number of FIR filter coefficients at 450, and where Fs is the sampling frequency (Hz). The baseline was estimated as a median of 10 s of inactivity one second before the peak. In a further step, the algorithm allowed manual inclusion or exclusion of identified transients. Mean transient frequencies (transients / min) were calculated using the arithmetic mean. Average response latencies upon 2-P optogenetic stimuli as well as average amplitudes of stimulation induced artifacts were determined by calculating arithmetic means. For quantification of the stimulus responses and the artifacts we

used a custom-made analysis algorithm which depicted the maximal dF / F_0 value of the calcium trace of cell within 10 frames before and 50 frames after a stimulus and averaged by calculating arithmetic means (usually 10-15 stimulations per cell). For artifact quantification extreme values exceeding $\pm$ 2 x SD were excluded. The fraction of responding cells was calculated by dividing the number of responding cells by the number of all stimulated cells. The rate of evoked calcium transients was calculated by dividing the number of evoked calcium transients by the total number of stimulation trials. The code for analysis can be found at: https://github.com/Strohlab.

Statistics. Inferential statistics was done with data sets with sample size of $n \geq 5$. Statistical significance was tested in GraphPad Prism. Significance levels were * $p < 0.05$, ** $p < 0.01$, *** $p < 0.001$ and **** $p < 0.0001$. For all data, we first tested for normality using the one-sample Kolmogorov-Smirnov test. In case that the null hypothesis (H_0) of a normal distribution could not be rejected (for $p > 0.05$), we employed a parametric test (t test), if H_0 could be rejected (for $p < 0.05$) we used a non-parametric test (Mann-Whitney U test). Data sets of Fig. S1 C (number of active cells) and D (number spontaneous calcium transients) where normalized to values at 920 nm (100 %). For quantification of the artifact we performed a non-linear regression and for testing the relationship of GCaMP's sensitivity and specificity we performed a linear regression analysis. Descriptive statistics given in the text are mean $\pm$ s.e.m. and error bars are displayed mean $\pm$ s.e.m.. Box-whisker plots are displayed 25 - 75 % (box) and 10 - 90 % percentile (whiskers). Statistical analysis and non-linear regression were performed using GraphPad Prism.

Supplemental References:

Arnoux, I., M. Willam, N. Griesche, J. Krummeich, H. Watari, N. Offermann, S. Weber, P. Narayan Dey, C. Chen, O. Monteiro, S. Buettner, K. Meyer, D. Bano, K. Radyushkin, R. Langston, J. J. Lambert, E. Wanker, A. Methner, S. Krauss, S. Schweiger and A. Stroh (2018). "Metformin reverses early cortical network dysfunction and behavior changes in Huntington's disease." Elife **7**.

Cardin, J. A., M. Carlen, K. Meletis, U. Knoblich, F. Zhang, K. Deisseroth, L. H. Tsai and C. I. Moore (2009). "Driving fast-spiking cells induces gamma rhythm and controls sensory responses." Nature **459**(7247): 663-667.

Packer, A. M., L. E. Russell, H. W. Dalgleish and M. Hausser (2015). "Simultaneous all-optical manipulation and recording of neural circuit activity with cellular resolution in vivo." Nat Methods **12**(2): 140-146.

Prakash, R., O. Yizhar, B. Grewe, C. Ramakrishnan, N. Wang, I. Goshen, A. M. Packer, D. S. Peterka, R. Yuste, M. J. Schnitzer and K. Deisseroth (2012). "Two-photon optogenetic toolbox for fast inhibition, excitation and bistable modulation." Nat Methods **9**(12): 1171-1179.